

A Novel Consistent-Robust SINS/GNSS/NHC Integrated Navigation Method for Autonomous Vehicles Under Intermittent GNSS Outage

Siyuan Du, Yulong Huang, *Senior Member, IEEE*, Weisong Wen, *Member, IEEE*, Yonggang Zhang, *Senior Member, IEEE*

Abstract—Autonomous vehicles are widely used in logistics, public transportation, and specialized industries, its high-precision navigation and positioning is predominantly supported through strapdown inertial navigation system/global navigation satellite system (SINS/GNSS) integrated navigation, thus ensuring safe and efficient operations. In practice, GNSS is prone to intermittent outage due to environment interference, while Non-Holonomic Constraint (NHC) can significantly improve navigation accuracy. Unfortunately, the mounting error angle and lever arm lead to NHC mismatch, and the performance of existing NHC method is also affected by the state-space model inconsistency and non-stationarity outlier noises. To solve the problems, a consistent-robust SINS/GNSS/NHC integrated navigation method is proposed, which includes two stages: off-line calibration and online navigation. In off-line calibration stage, a two-step-based estimation method is proposed to determine the mounting error angle and lever arm. The more consistent state-space model is deduced to estimate mounting error angle using the virtual dead-reckoning constructed from the posteriori straight-driving data, based on which the lever arm can be accurately estimated using posterior turn-driving data. In online navigation stage, the Lie group-based NHC model is established, and the non-stationary outlier noise is modeled as Gaussian-Student's t mixture distribution. Meanwhile, the strong tracking method is introduced to fine-calibrate the accuracy of initial parameter. Finally, the variational Bayesian is used to jointly estimate the navigation state and parameters. The simulation and car-mounted field test results illustrate that the proposed method has better estimation accuracy than existing state-of-the-art methods, enhancing the navigation and positioning capabilities of autonomous vehicles during intermittent GNSS outage.

Index Terms—Autonomous vehicles, integrated navigation, GNSS outage, Non-holonomic constraint, Lie group, variational Bayesian, robust filtering

I. INTRODUCTION

Autonomous vehicles have been widely applied in areas such as logistics, public transportation, and specialized industries [1]. The accurate navigation and positioning are crucial for the motion planning and control of autonomous vehicles [2], [3]. In addition, accurate navigation and positioning is also the first condition to ensure the safety of autonomous vehicles

This work was supported in part by the National Natural Science Foundation of China under Grant 62373118 and Grant 62173105. (Corresponding author: Yulong Huang.)

S. Du, Y. Huang and Y. Zhang are with the College of Intelligent Systems Science and Engineering, Harbin Engineering University, Harbin 150001, China (e-mail: dusy@hrbeu.edu.cn; heuedu@163.com; zhangyg@hrbeu.edu.cn).

W. Wen is with Department of Aeronautical and Aviation Engineering, Hong Kong Polytechnic University, Hong Kong (e-mail: Weisong.wen@polyu.edu.hk).

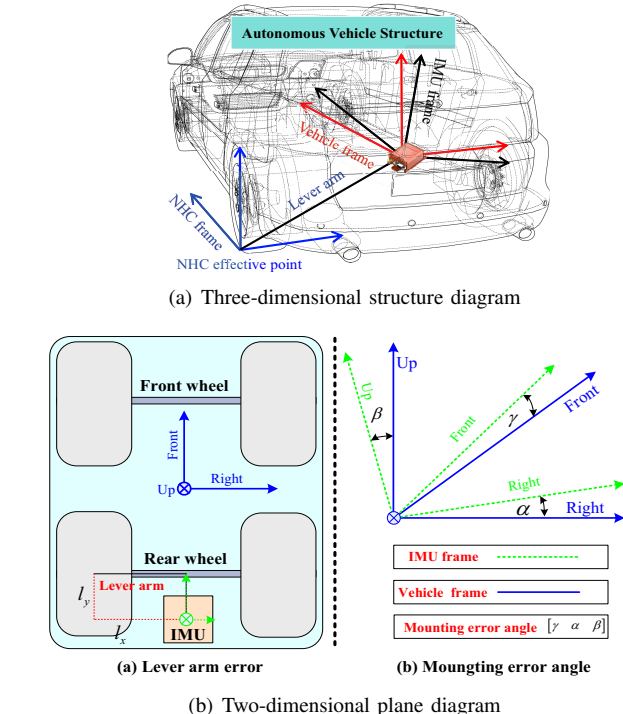


Fig. 1: Schematic of NHC mounting error angle and lever arm¹

[4]. Since the strapdown inertial navigation system/global navigation satellite system (SINS/GNSS) integrated navigation can achieve continuous and high-precision navigation, it is widely used in most autonomous vehicles [5]–[7], and Micro-Electro-Mechanical System (MEMS)-based SINS is often used as the main navigation system [8], [9]. However, when autonomous vehicles are in environments such as tunnels, forests, and valleys, GNSS often experiences intermittent outage, which makes it difficult for MEMS-based SINS to maintain high-precision navigation [10], [11].

As a low-cost way, the Non-Holonomic Constraint (NHC) method can improve navigation accuracy with relatively low complexity and technical obstacles for autonomous vehicles with intermittent GNSS outage. The NHC is based on the driving characteristics of vehicle, i.e., the horizontal and vertical velocities of autonomous vehicle are theoretically zero, which

¹The mounting error angle $[\gamma, \alpha, \beta]$ is the deviation angle between the IMU frame and the vehicle frame. The lever arm $\mathbf{I}_{\text{NHC}} = [l_x, l_y, l_z]$ is the distance between the IMU frame center point and the NHC effective point.

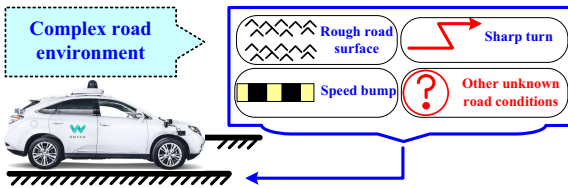


Fig. 2: Non-stationary outlier noises caused by the complex road environment.

can be used as the measurement to correct navigation errors [27]. This principle is closely related to the concept of dynamic zero velocity update (DZUPT), and NHC is often specifically referred to as DZUPT. However, as shown in 1, when the vehicle climbs, turns or changes lanes, the mounting error angle and the lever arm will cause NHC mismatch problem, which will reduce the accuracy of the NHC-based integrated navigation [28]–[30]. Therefore, if the mounting error angle and lever arm are accurately compensated, the best frame and effective point of NHC can be guaranteed. In addition, the performance of existing NHC method is also limited. On one hand, the accuracy of existing NHC measurement model is affected by the inaccurate navigation state, especially the attitude matrix. If the estimated attitude is not accurate, the estimation consistency of NHC measurement model is poor. On the other hand, the reliability of NHC is compromised by the complex road environment, including sideslip from sharp turn or speed bump, bounce from rough road surface, and other non-standardized traffic conditions, as shown in Fig. 2. These unpredictable conditions prone to cause non-stationary outlier noises in NHC measurements, i.e., the noise may be Gaussian distribution in one time period and thick-tailed distribution in another. Although existing NHC method have a certain role in enhancing the navigation accuracy of autonomous vehicles during intermittent GNSS outage, it remains a challenge to achieve long-term stability in complex road conditions.

Based on the above analyses, the problems of existing NHC method can be summarized as the NHC mismatch caused by the mounting error angle and lever arm, and limited NHC performance caused by the model inconsistency and non-stationary outlier noise uncertainty. Therefore, to realize the maximum potential of NHC method in autonomous vehicles, it is necessary to explore more consistent and robust efficient algorithm. In this paper, a novel consistent-robust SINS/GNSS/NHC integrated navigation method is proposed, which mainly includes off-line calibration stage and online navigation stage, as shown in Fig. 3. In off-line calibration stage, a two-step-based method is proposed to accurately estimate the mounting error angle and lever arm, which solves the NHC mismatch problem. In step-one, an invariant extended Kalman filter (IEKF)-based virtual-dead rocking (VDR) method is proposed in Lie group (LG) framework based on the posteriori straight-driving data and VDR scheme. Compared with the existing extended Kalman filter (EKF)-based VDR method [29], the proposed IEKF-based VDR method has better consistency in estimating the mounting error angle. Subsequently, in step-two, the lever arm can be easily estimated by Kalman filter (KF) method using the

estimated mounting error angle and posteriori turn-driving data. In online navigation stage, an improved Gaussian-Student's t mixture(GSTM)-based variational Bayesian (VB) robust filtering is proposed, which is used to solve the problem of NHC model inconsistency and non-stationary outlier noise uncertainty. Compared with the existing NHC state-space model (SSM), the proposed LG-based NHC SSM exhibits better state independence and estimation consistency. Moreover, the proposed improved robust filtering models the non-stationary outlier noise as the GSTM distribution and uses the VB method to estimate the state and parameters. Meanwhile, in order to make the proposed robust filtering more sensitive to potential uncertainties, the strong tracking method is introduced in the initial measurement update to fine-calibrate the nominal measurement covariance matrix, i.e., the nominal measurement covariance matrix is adjusted by a dynamic parameter. In conclusions, the contributions of this paper are summarized as follows:

- To solve the NHC mismatch problem, a two-step-based offline calibration method is proposed. In step-one, the IEKF-based VDR method is proposed to estimate the mounting error angle. Subsequently, in step-two, the NHC lever arm is further estimated based on the estimated mounting error angle.
- To improve the performance of NHC estimation method, a novel LG-based consistent NHC model is constructed. On that basis, an improved GSTM-based VB robust filtering is proposed to solve the problem of non-stationary outlier noise caused by complex road environment.
- Simulations and car-mounted field experiments demonstrate that, in the case of intermittent GNSS outage, the proposed consistent-robust SINS/GNSS/NHC integrated navigation method has higher convergence accuracy than existing cutting-edge methods.

The remain of this paper is organized as follows. The related works are presented in Section II. The problem and motivation of existing HNC method are given in Section III. In Section IV, a two-step-based method is proposed to solve the NHC mismatch problem. In Section V, a novel LG-based NHC SSM is derived, based on which, an improved GSTM-based VB robust filtering is proposed to solve the NHC non-stationary outlier noises. In Sections VI and VII, the performance of the proposed method is compared with that of existing methods through simulations and car-mounted field tests, respectively. Conclusions are drawn in Section VIII.

II. RELATED WORK

For the intermittent GNSS outage, there are some researchers have already been proposed, which can be summarized as the multi-sensor-based integrated navigation method, the artificial neural network (ANN)-based integrated navigation method, and the kinematic constraint-based integrated navigation method. For the multi-sensor-based integrated navigation method, the solution is to add auxiliary sensors, such as magnetometer [12], Lidar [13], [14], visual odometers [15], [16], etc. Correspondingly, the multi-sensor-based integrated navigation system can continue to provide other types of

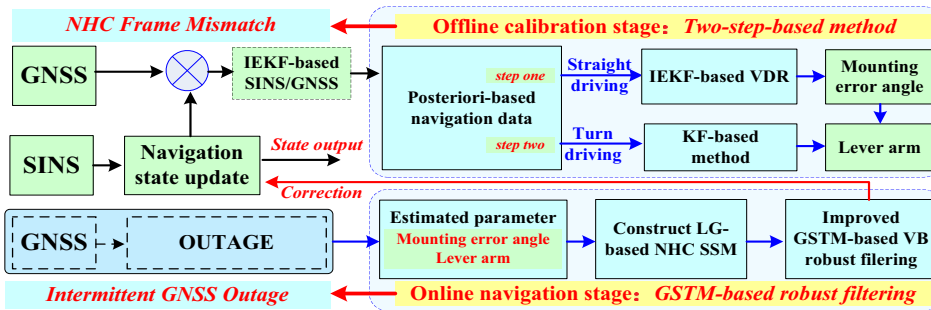


Fig. 3: Diagram of the proposed SINS/GNSS/NHC integrated navigation algorithm structure.

measurements during intermittent GNSS outage. However, the additional sensors will inevitably increase the cost of navigation system and also increase the complexity of algorithm operation. For the ANN-based integrated navigation method, the solution is to use the ANN model to correct the SINS errors during intermittent GNSS outage [17]–[21]. In addition, it includes the training mode and the predictive output mode, respectively. In the training mode, its heart task is to construct a generalized nonlinear equation between the model input and the predicted output. Generally, the gyroscope angular rate, accelerometer specific force, and SINS navigation state are commonly used as model inputs. The predicted outputs are the GNSS measurement or estimated state error variable. Then, when GNSS experiences intermittent outage, the prediction output mode utilizes the model trained in the training mode to predict GNSS measurement or estimated state error variable. However, the ANN-based method has the problems of high computational complexity, low operating reliability, and weak generalization ability. For the kinematic constraint-based integrated navigation method, its core is to utilize natural auxiliary information to correct SINS errors during intermittent GNSS outage. By contrast, it is especially easy to implement without adding auxiliary sensors [22], [23]. In general, the existing kinematic constraint-based methods include the zero velocity update (ZUPT) [24], the zero angular rate update (ZARU) [25], and the zero integrated heading rate (ZIHR) [26], etc. Theoretically, when the autonomous vehicles remain stationary, the output velocity, gyroscope angular rate, and heading of the MEMS-based SINS remain unchange. Consequently, ZUPT, ZARU, and ZIHR can be used to correct the navigation errors, respectively. However, these methods all require to remain stationary for a period of time, which limits the maneuvering ability of the autonomous vehicles. In contrast, the NHC method is based on the driving characteristics of the autonomous vehicles, i.e., its velocity in both horizontal and vertical directions can be used as the measurement to correct navigation errors during intermittent GNSS outage. Furthermore, the NHC method ensures real-time navigation. However, due to the mounting angle and lever arm, the NHC suffers from mismatch, i.e., the assumed frame and effective point of NHC are suboptimal.

The existing mounting error angle estimation method can be summarized as the acceleration-based observation method [32], velocity-based observation method [33], and position-based observation method [29]. For the acceleration-based

observation method, the mounting error angle is calculated indirectly through the projection deviation angle between the horizontal and vertical directions of the SINS acceleration. For the velocity-based observation method, the mounting error angle is set as estimated state of the filter, and the velocity difference between odometer and SINS is taken as the measurement to estimate the mounting error angle. However, the estimation accuracy of these methods largely depends on the quality of measurement vectors and is not suitable to low-precision MEMS-based SINS. By contrast, it has been proved that the position-based observation method is better than others [29], which is specifically named as EKF-based VDR method. The core idea is to utilize the posteriori SINS/GNSS results to construct VDR scheme strictly satisfying NHC, and then derive the differential equation of the mounting error angle. In addition, the EKF-based VDR is actually an offline method. It utilizes the position difference between the VDR-indicated position and the posteriori SINS/GNSS position as the measurement innovation to estimate the mounting error angle. However, the derived VDR-indicated position is affected by the attitude error, which reduces the estimation accuracy of the mounting error angle. Compared with the estimation of mounting error angle, the NHC lever arm is easily estimated for the reason of observability, which can be summarized as KF-based method and Least square(LS)-based method. However, both KF-based and LS-based methods need to ensure the accurate estimated mounting error angle in advance [30]. Therefore, in order to estimate the mounting error angle and lever arm more accurately, a two-step-based off-line calibration method is proposed in this paper. Compared with the existing EKF-based VDR method, the proposed IEKF-based VDR method has better estimation consistency in the mounting error angle. Subsequently, based on the estimated mounting error angle, the modified lever arm error measurement model can be further optimized to ensure its estimation accuracy and stability.

In addition to the NHC mismatch problem, the performance of the existing NHC-based method is also limited. The inaccurate navigation states affect the NHC model and thus reduce the estimation consistency of the filter. Moreover, the existing NHC methods also require further improvements to address the effects of non-stationary measurement outliers noise generated by rapidly changing road conditions, non-standard traffic situations, and other unknown environmental disturbances. Although artificially setting empirical NHC measurement covariance can enhance estimation accuracy to

Nomenclatures and Notions

Notations	Definitions
i	Earth-Centered Inertial frame.
b	Right-Front-Up body frame (same with IMU frame).
e	Earth-Centered-Earth-Fixed frame.
n	East-North-Up local navigation frame.
u	Right-Front-Up vehicle frame.
ω_{ie}	Earth rotation rate.
ω_{xy}^z	Rotation rate of y frame with respect to x frame, and project on z frame.
$SO(3)$	Group of rotation matrices.
$SE_2(3)$	Group of double direct isometries.
I_n	$n \times n$ identity matrix.
0_n	$n \times n$ zero matrix.
$0_{n \times m}$	$n \times m$ matrix or vector.
$N(\cdot; \mu, \Sigma)$	Gaussian probability density function with mean μ and covariance Σ .
$St(\cdot; \mu, \Sigma, v)$	Gaussian distribution with mean μ and covariance Σ .
$G(\cdot; x, y)$	Student's t probability density function with mean μ , scale matrix Σ , and dof parameter v .
$(\cdot)^{-1}$	Gamma probability density function with shape parameter x and rate parameter y .
$(\cdot)^T$	Inverse operation.
$(\cdot)^i$	Transpose operation.
$(\cdot)^{\times}$	Calculation results of the i th-iteration.
$E[\cdot]$	Skew symmetric matrix.
$tr(\cdot)$	Expectation operator.
$\text{J}(\phi)$	Matrix trace operation.
	Jacobian matrix of ϕ , and approximately equal to $I_3 + 0.5(\phi \times)$.

some extent, it still fails to adapt the complex dynamic environments. In addition, to resist outliers noise, the Huber-based KF [34] and maximum correntropy KF [35] are both designed. However, some useful random information is omitted in this process, which weakens the filtering accuracy. By contrast, although the fixed scale and freedom parameter-based robust Student's t Kalman filtering (RSTKF) takes into account the random characteristics of heavy-tailed noise, the estimation accuracy is poor under the non-stationary outlier noise [36]. In this paper, to realize the maximum potential of the NHC method, Lie group framework is first introduced to the existing NHC for consistency improvement. Then, in the framework of VB, the non-stationary outlier noises are modeled as GSTM distribution, so as to better capture the noise characteristics in complex road environment. In addition, the strong tracking method is used to fine-calibrate the initial measurement covariance matrix, which further strengthens the adaptability to dynamic uncertainties. This paper offers a new perspective for the application of NHC method, significantly enhancing the navigation accuracy and reliability of autonomous vehicles during intermittent GNSS outage.

III. PROBLEM FORMULATIONS

In this section, we further analyze the problems of the existing mounting error angle and lever arm estimation method and the existing NHC-based integrated navigation method. Then, the corresponding research motivation and solutions are given, respectively.

A. Problems of mounting error angle and the lever arm estimates

For the existing EKF-based VDR method, its core is to construct a mounting error angle-based Dead Rocking process

by using posteriori SINS/GNSS straight-driving data. For the u -frame autonomous vehicle, the incremental distance Δs_k^u is defined as [29]

$$\Delta s_k^u = \int_{t_{k-1}}^{t_k} \mathbf{v}^u(t) dt \quad (1)$$

where the dt denotes the resample cycle time, and the incremental distance $\Delta s_k^u = [\Delta s_k, 0, 0]$, and $\mathbf{v}^u(t) = [v^u, 0, 0]$ denotes the u -frame velocity of autonomous vehicle, and it is formulated as follows

$$v^u = \sqrt{\hat{v}_F^2 + \hat{v}_R^2 + \hat{v}_D^2} \quad (2)$$

where \hat{v}_F , \hat{v}_R , and \hat{v}_D denote the b frame velocity of front, right, and down, respectively, which is different from the definition in this paper. And they can be obtained from the posteriori SINS/GNSS navigation data. Actually, (2) forces $\mathbf{v}^u(t)$ to satisfy the NHC criterion. In addition, $\Delta s_k = v^u dt$. However, due to the mounting error angle, the b frame is misaligned with the u frame. Therefore, the VDR position $\mathbf{r}_{\text{vdr}}^n$ update equation can be further obtained as follows

$$\mathbf{r}_{\text{vdr},k}^n = \mathbf{r}_{\text{vdr},k-1}^n + \mathbf{C}_b^n \mathbf{C}_u^b \Delta s_k^u \quad (3)$$

where \mathbf{C}_b^n denotes the attitude rotation matrix, and \mathbf{C}_b^u denotes the mounting error angle matrix. Then, based on (3), the corresponding state error equation and measurement error equation are formulated as follows [29].

$$\delta \mathbf{x}_k = \Phi_{k|k-1} \delta \mathbf{x}_{k-1} + \mathbf{G}_{k-1} \boldsymbol{\varpi}_{k-1} \quad (4)$$

$$\delta \mathbf{z}_k = \mathbf{H}_{\text{vdr},k} \delta \mathbf{x}_k + \boldsymbol{\nu}_{\text{vdr},k} \quad (5)$$

where

$$\Phi_{k|k-1} = \begin{bmatrix} I_3 & -\mathbf{C}_b^n \mathbf{C}_u^b \mathbf{M} & \Delta s_k^n \times \\ \mathbf{0}_2 & I_2 & \mathbf{0}_2 \\ \mathbf{0}_3 & \mathbf{0}_3 & I_3 \end{bmatrix}, \mathbf{G}_{k-1} = \begin{bmatrix} \mathbf{0}_{3 \times 5} \\ \mathbf{I}_5 \end{bmatrix} \quad (6)$$

and

$$\mathbf{M} = \begin{bmatrix} 0 & 0 \\ 0 & -\Delta s_k \\ \Delta s_k & 0 \end{bmatrix}, \Delta s_k^n = \mathbf{C}_b^n \mathbf{C}_u^b \Delta s_k^u, \mathbf{H}_{\text{vdr},k} = \begin{bmatrix} I_3 \\ \mathbf{0}_3 \\ \mathbf{0}_3 \end{bmatrix}^T \quad (7)$$

where $\delta \mathbf{x}_k = [\delta \mathbf{r}^n, \alpha, \phi^n]^T$ denote the position state error, mounting error angle, and misalignment angle, respectively, and $\boldsymbol{\varpi}_{k-1}$ and $\boldsymbol{\nu}_{\text{vdr},k}$ denote the Gaussian white noise, and Δs_k is calculated by (1)-(2). In addition, the measurement innovation $\delta \mathbf{z}_k$ is formulated as [29]

$$\delta \mathbf{z}_k = \hat{\mathbf{r}}_k^n - \tilde{\mathbf{r}}_k^n \quad (8)$$

where $\hat{\mathbf{r}}_k^n$ denotes the updated VDR-indicated position vector in (3), and $\tilde{\mathbf{r}}_k^n$ denotes the posteriori SINS/GNSS position vector. For the existing EKF-based VDR method, the state transition matrix $\Phi_{k|k-1}$ is mainly composed of \mathbf{C}_b^n , \mathbf{C}_u^b , \mathbf{M} , and Δs_k^n . On one hand, \mathbf{M} is derived from the posteriori data in (1)-(2), thereby introducing velocity related errors to a certain extent. On the other hand, the increment Δs_k^n is derived from $\mathbf{C}_b^n \mathbf{C}_u^b \Delta s_k^u$. It indicates that the accuracy of state transition matrix $\Phi_{k|k-1}$ essentially determined by \mathbf{C}_b^n and \mathbf{C}_u^b . In other words, \mathbf{C}_b^n and \mathbf{C}_u^b will directly affect the estimation consistency of the mounting error angle by affecting the state

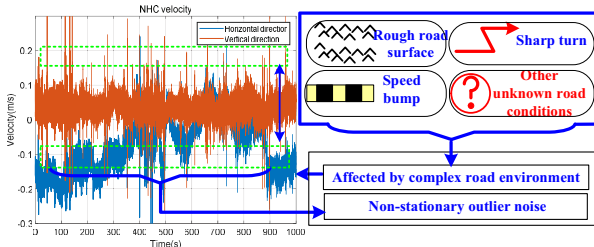


Fig. 4: The NHC non-stationary outlier noise².

transition matrix. Although \mathbf{C}_b^n is obtained from posteriori SINS/GNSS navigation state, its accuracy is highly dependent on the performance of the SINS/GNSS integrated navigation system. In addition, the NHC lever arm is considered the distance between the central point of the IMU and the effective point of the NHC. Then, when the autonomous vehicle turns, its NHC innovation vector is formulated as [30]

$$\delta \mathbf{z}_{\text{nhc}}^u = \mathbf{C}_b^u \mathbf{C}_n^b \mathbf{v}_{\text{imu}}^n + \mathbf{C}_b^u (\omega_{nb}^b \times \mathbf{l}^b) \quad (9)$$

where \mathbf{l}^b denotes the lever arm, and ω_{nb}^b denotes the angular rate of frame b relative to the frame n . Based on (9), the lever arm error $\delta \mathbf{l}^b$ measurement matrix \mathbf{H}_{la} is formulated as [30]

$$\mathbf{H}_{\text{la}} = [\mathbf{C}_b^u (\omega_{nb}^b \times)] \quad (10)$$

For the measurement matrix in (10), it indicates that if the mounting error angle matrix \mathbf{C}_b^u and angular rate ω_{nb}^b are inaccurate, the lever arm error $\delta \mathbf{l}^b$ will not be accurately estimated.

B. Problems of existing NHC-based integrated navigation method

In order to analyze the problems of existing NHC-based integrated navigation method, the existing NHC measurement equation is formulated as [40]

$$\delta \mathbf{v}_{\text{nhc}}^u = \mathbf{C}_b^u (\mathbf{C}_n^b \delta \mathbf{v}_{\text{sins}}^n - \mathbf{C}_n^b (\mathbf{v}_{\text{sins}}^n \times) \phi^n - (\mathbf{l}^b \times) \delta \omega_{ib}^b) + \nu_{\text{nhc}} \quad (11)$$

where ϕ^n , $\delta \mathbf{v}_{\text{sins}}^n$, and $\delta \omega_{ib}^b$ denote the state error of misalignment, velocity, and gyroscope bias, respectively, and ν_{nhc} denotes the NHC measurement noise. Then, the NHC measurement matrix \mathbf{H}_{nhc} is given by:

$$\mathbf{H}_{\text{nhc}} = \begin{bmatrix} \mathbf{h}_{\{1,1\}} & \mathbf{h}_{\{1,2\}} & \mathbf{0}_{1 \times 3} & -\mathbf{C}_b^u (\mathbf{l}^b \times) (1,:) & \mathbf{0}_{1 \times 3} \\ \mathbf{h}_{\{2,1\}} & \mathbf{h}_{\{2,2\}} & \mathbf{0}_{1 \times 3} & -\mathbf{C}_b^u (\mathbf{l}^b \times) (3,:) & \mathbf{0}_{1 \times 3} \end{bmatrix} \quad (12)$$

where

$$\begin{cases} \mathbf{h}_{\{1,1\}} = -\mathbf{C}_b^u \mathbf{C}_n^b (\mathbf{v}_{\text{sins}}^n \times) (1,:), \mathbf{h}_{\{1,2\}} = \mathbf{C}_b^u \mathbf{C}_n^b (1,:) \\ \mathbf{h}_{\{2,1\}} = -\mathbf{C}_b^u \mathbf{C}_n^b (\mathbf{v}_{\text{sins}}^n \times) (3,:), \mathbf{h}_{\{2,2\}} = \mathbf{C}_b^u \mathbf{C}_n^b (3,:) \end{cases} \quad (13)$$

where $\{\cdot\}(x,:)$ denotes the x -th row of matrix $\{\cdot\}$. For the measurement matrix \mathbf{H}_{nhc} , it is not only related to the mounting error angle \mathbf{C}_b^u and lever arm \mathbf{l}^b , but also to the navigation attitude \mathbf{C}_b^n and velocity $\mathbf{v}_{\text{sins}}^n$. Therefore, the former errors will lead to NHC mismatch problem, while the latter errors will lead to NHC estimation inconsistency problem.

²The results are from the car-mounted filed test in Section VIII.

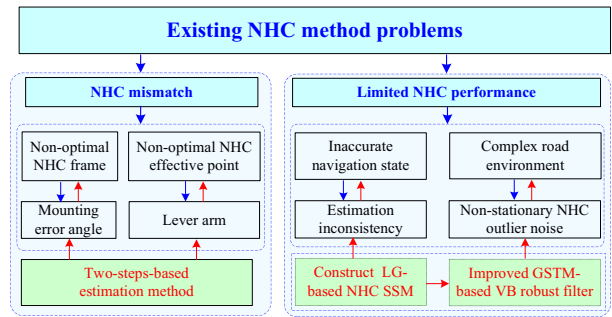


Fig. 5: Challenges analyses and proposed solutions.

Additionally, influenced by complex road environments, the NHC measurement noise actually does not conform strictly to a Gaussian distribution. As shown in Fig. 4, on one hand, the NHC measurement noises in red and blue exhibit a small constant value influenced by the NHC mismatch. On the other hand, as indicated by the dashed square, the NHC measurement noises actually exhibit the non-stationary outlier property, i.e., at certain times, it may conform to a Gaussian distribution, while at other times, it may exhibit a heavy-tailed distribution. Although the existing Student's t robust filtering based on the fixed scale and freedom parameter can resist outlier noise to some extent, it can not accurately model the non-stationary distribution, so the estimation accuracy is poor.

Motivated by the above analyses, we address challenges on two fronts, as shown in Fig. 5. On one hand, due to the mounting error angle and lever arm, it is impossible to ensure the optimal NHC frame and effective NHC point. Correspondingly, a two-step-based offline calibration estimation method is proposed. In step-one, based on the posteriori SINS/GNSS straight-driving data, an novel IEKF-based VDR method is constructed to estimate mounting error angle in a more consistent manner. Subsequently, in step-two, based on the estimated mounting error angle and posteriori SINS/GNSS turn-driving data, the modified lever arm error measurement equation is constructed, and then the lever arm error is estimated accurately. On the other hand, the inaccurate navigation states can affect the estimation consistency of the NHC model, and the complex road environments can cause NHC non-stationary outlier noises. Therefore, firstly, the LG-based NHC SSM is constructed to improve the estimation consistency. Then, the non-stationary outlier noise is modeled as GSTM distribution, and the strong tracking method is used to fine-calibrate the accuracy of initial nominal measurement covariance matrix. Finally, the VB method realize the joint estimate of state errors and parameters during intermittent GNSS outage.

IV. THE PROPOSED TWO-STEP-BASED METHOD FOR ESTIMATING MOUNTING ERROR ANGLE AND LEVER ARM

A. The definitions of LG-based invariant error

In the navigation and positioning of autonomous Vehicles, the attitude rotation matrix \mathbf{R} , velocity vector \mathbf{v} , and position vector \mathbf{r} actually belong to $SE_2(3)$, which is represented as

follows [38], [39]

$$\chi \triangleq \begin{bmatrix} \mathbf{R} \in SO(3) & \mathbf{v} \in \mathbb{R}^3 & \mathbf{r} \in \mathbb{R}^3 \\ \mathbf{0}_{1 \times 3} & 1 & 0 \\ \mathbf{0}_{1 \times 3} & 0 & 1 \end{bmatrix} \in SE_2(3) \quad (14)$$

For the definition of left invariant error $[\phi^b, \zeta_v^L, \zeta_r^L]$, it can be transformed from the left group error $\delta\chi^L$, which is given by [38], [39]

$$\begin{aligned} \delta\chi^L &= \tilde{\chi}^{-1}\chi = \begin{bmatrix} \tilde{\mathbf{R}}^T \mathbf{R} & \tilde{\mathbf{R}}^T(\mathbf{v} - \tilde{\mathbf{v}}) & \tilde{\mathbf{R}}^T(\mathbf{r} - \tilde{\mathbf{r}}) \\ \mathbf{0}_{1 \times 3} & 1 & 0 \\ \mathbf{0}_{1 \times 3} & 0 & 1 \end{bmatrix} \\ &= \begin{bmatrix} \exp_G(\phi^b \times) & \mathbf{J}(\phi^b) \zeta_v^L & \mathbf{J}(\phi^b) \zeta_r^L \\ \mathbf{0}_{1 \times 3} & 1 & 0 \\ \mathbf{0}_{1 \times 3} & 0 & 1 \end{bmatrix} \end{aligned} \quad (15)$$

where

$$\exp_G(\phi^b \times) = \tilde{\mathbf{R}}^T \mathbf{R} \approx \mathbf{I}_3 + \phi^b \times \quad (16)$$

$$\mathbf{J}(\phi^b) \zeta_v^L = \tilde{\mathbf{R}}(\mathbf{v} - \tilde{\mathbf{v}}) = -\tilde{\mathbf{R}} \delta\mathbf{v} \quad (17)$$

$$\mathbf{J}(\phi^b) \zeta_r^L = \tilde{\mathbf{R}}(\mathbf{r} - \tilde{\mathbf{r}}) = -\tilde{\mathbf{R}} \delta\mathbf{r} \quad (18)$$

Similarly, for the definition of right invariant error $[\phi^n, \zeta_v^R, \zeta_r^R]$, it can be transformed from the right group error $\delta\chi^R$, which is given by [38], [39]

$$\begin{aligned} \delta\chi^R &= \chi \tilde{\chi}^{-1} = \begin{bmatrix} \mathbf{R} \tilde{\mathbf{R}}^T & \mathbf{v} - \mathbf{R} \tilde{\mathbf{R}}^T \tilde{\mathbf{v}} & \mathbf{r} - \mathbf{R} \tilde{\mathbf{R}}^T \tilde{\mathbf{r}} \\ \mathbf{0}_{1 \times 3} & 1 & 0 \\ \mathbf{0}_{1 \times 3} & 0 & 1 \end{bmatrix} \\ &= \begin{bmatrix} \exp_G(\phi^n \times) & \mathbf{J}(\phi^n) \zeta_v^R & \mathbf{J}(\phi^n) \zeta_r^R \\ \mathbf{0}_{1 \times 3} & 1 & 0 \\ \mathbf{0}_{1 \times 3} & 0 & 1 \end{bmatrix} \end{aligned} \quad (19)$$

where

$$\exp_G(\phi^n \times) = \mathbf{R} \tilde{\mathbf{R}}^T \approx \mathbf{I}_3 + \phi^n \times \quad (20)$$

$$\mathbf{J}(\phi^n) \zeta_v^R = \mathbf{v} - \mathbf{R} \tilde{\mathbf{R}}^T \tilde{\mathbf{v}} = -\delta\mathbf{v} + \tilde{\mathbf{v}} \times \phi^n \quad (21)$$

$$\mathbf{J}(\phi^n) \zeta_r^R = \mathbf{r} - \mathbf{R} \tilde{\mathbf{R}}^T \tilde{\mathbf{r}} = -\delta\mathbf{r} + \tilde{\mathbf{r}} \times \phi^n \quad (22)$$

B. The proposed two-step-based estimation method

In step-one, the VDR position update equation are constructed by the posteriori straight-driving data, which strictly meets the NHC criteria. Subsequently, based on the constructed VDR scheme and the Lie group framework, the right invariant error differential equation is derived and the corresponding consistency SSM is obtained. Meanwhile, the measurement equation is constructed using the difference between the posteriori straight-driving position and the VDR update position. Finally, the mounting error angle can be accurately estimated by IEKF method. In addition, according to the definition of invariant error, the right invariant extended Kalman filter (RIEKF) and left invariant extended Kalman filter (LIEKF) can be obtained, respectively. In the following **Theorem1**, the corresponding derivation process of the proposed RIEKF-based VDR method is given.

Theorem 1. *In the proposed RIEKF-based VDR method, the SSM includes state and measurement equations based on right*

invariant error, and the right invariant error can be defined as

$$\mathbf{x}_{\text{ma}}^R = [\zeta_{\text{ma}}^R, \alpha_{\text{ma}}, \phi_{\text{ma}}^n]^T \quad (23)$$

where ζ_{ma}^R , α_{ma} , and ϕ_{ma}^n denote the right invariant position error, the mounting error angle, and misalignment angle, respectively, and the right invariant error-based state equation is given by

$$\mathbf{x}_{\text{ma},k|k-1}^R = \Phi_{k|k-1}^R \mathbf{x}_{\text{ma},k-1}^R + \Gamma_{k-1}^R \boldsymbol{\sigma}_{\text{ma}} \quad (24)$$

where

$$\Phi_{k|k-1}^R = \begin{bmatrix} \mathbf{I}_3 & \mathbf{C}_b^n \mathbf{C}_u^b \mathbf{M}^R & \mathbf{0}_3 \\ \mathbf{0}_2 & \mathbf{I}_2 & \mathbf{0}_2 \\ \mathbf{0}_3 & \mathbf{0}_3 & \mathbf{I}_3 \end{bmatrix}, \Gamma_{k-1}^R = \begin{bmatrix} \mathbf{0}_{3 \times 5} \\ \mathbf{I}_5 \end{bmatrix} \quad (25)$$

where $\boldsymbol{\sigma}_{\text{ma}}$ denote the Gaussian noise, i.e., $\boldsymbol{\sigma}_{\text{ma}} \sim \mathcal{N}(\mathbf{0}, \mathbf{Q}_{\text{ma}})$, and \mathbf{M}^R is given by

$$\mathbf{M}^R = \begin{bmatrix} 0 & \Delta s_k \\ 0 & 0 \\ -\Delta s_k & 0 \end{bmatrix} \quad (26)$$

where $\Delta s_k = v^u dt$, and the right invariant error-based VDR measurement equation is given by

$$\mathbf{z}_{\text{ma},k}^R = \mathbf{H}_{\text{ma}}^R \mathbf{x}_{\text{ma},k|k-1}^R + \boldsymbol{\nu}_{\text{ma}}^R \quad (27)$$

where $\boldsymbol{\nu}_{\text{ma}}^R$ denotes Gaussian noise, i.e., $\boldsymbol{\nu}_{\text{ma}}^R \sim \mathcal{N}(\mathbf{0}, \mathbf{R}_{\text{ma}})$, and the measurement innovation $\mathbf{z}_{\text{ma},k}^R$ and the measurement matrix \mathbf{H}_{ma}^R are formulated as follows, respectively

$$\begin{aligned} \mathbf{z}_{\text{ma},k}^R &= \mathbf{r}_{\text{vdr},k}^n - \mathbf{r}_{\text{sins/gnss},k}^n \\ \mathbf{H}_{\text{ma}}^R &= \left[-\mathbf{I}_3 \ \mathbf{0}_{3 \times 2} \ \left(\mathbf{r}_{\text{vdr},k}^n \times \right) \right] \end{aligned} \quad (28)$$

where $\mathbf{r}_{\text{sins/gnss},k}^n$ is derived from the posteriori navigation data, and $\mathbf{r}_{\text{vdr},k}^n$ is calculated as follows

$$\mathbf{r}_{\text{vdr},k}^n = \mathbf{r}_{\text{vdr},k-1}^n + \mathbf{C}_b^n \mathbf{C}_u^b \Delta \mathbf{s}_k^u \quad (29)$$

Proof: See Appendix A.

Remark 1. *Compared with the existing EKF-based VDR method, the state transition matrix $\Phi_{k|k-1}^R$ of the proposed RIEKF-based VDR method does not include $\mathbf{C}_b^n \mathbf{C}_u^b \Delta \mathbf{s}_k^u$, as shown in (6) and (25). As a result, the recursive error $\Delta \mathbf{s}_k^u$ will not affect the accuracy of $\Phi_{k|k-1}^R$, that is, the influences of the $\tilde{\mathbf{C}}_b^n$ and $\tilde{\mathbf{C}}_u^b$ to the state transition matrix $\Phi_{k|k-1}^R$ are accordingly reduced to some extent. Although the proposed RIEKF-based VDR method cannot achieve complete state independence, it still reduces the state independence to certain extent and improves the estimation consistency to the mounting error angle. In addition, according to the definition of invariant error, the LIEKF-based VDR method can also be derived. However, after detailed analyses, it can be concluded that the state independence of LIEKF-based VDR method is also worse than that of the proposed RIEKF-based VDR method. Therefore, in this paper, we only focus on the proposed RIEKF-based VDR method, while the less effective LIEKF-based VDR method is only used as a comparative reference.*

Based on the proposed SSM in (24)-(28), the mounting error angle can be estimated by the KF framework. Correspondingly the time update and measurement update are formulated as follows.

a) Time update:

$$\begin{aligned} \mathbf{x}_{\text{ma},k|k-1}^R &= \Phi_{k|k-1}^R \mathbf{x}_{\text{ma},k-1}^R \\ \mathbf{P}_{k|k-1} &= \Phi_{k|k-1}^R \mathbf{P}_{k-1} (\Phi_{k|k-1}^R)^T + \Gamma_{k-1}^R \mathbf{Q}_{\text{ma},k-1} (\Gamma_{k-1}^R)^T \end{aligned} \quad (30)$$

b) Measurement update:

$$\begin{aligned} \mathbf{K}_k &= \mathbf{P}_{k|k-1} (\mathbf{H}_{\text{ma},k}^R)^T (\mathbf{H}_{\text{ma},k}^R \mathbf{P}_{k|k-1} (\mathbf{H}_{\text{ma},k}^R)^T + \mathbf{R}_{\text{ma},k})^{-1} \\ \mathbf{x}_{\text{ma},k|k}^R &= \mathbf{x}_{\text{ma},k|k-1}^R + \mathbf{K}_k (\mathbf{z}_{\text{ma},k}^R - \mathbf{H}_{\text{ma},k}^R \mathbf{x}_{\text{ma},k|k-1}^R) \\ \mathbf{P}_{k|k} &= (\mathbf{I}_8 - \mathbf{K}_k \mathbf{H}_{\text{ma},k}^R) \mathbf{P}_{k|k-1} \end{aligned} \quad (31)$$

where $\mathbf{P}_{k|k-1}$ and $\mathbf{P}_{k|k}$ denote the one-step prediction error covariance matrix and posterior error covariance matrix, respectively, and \mathbf{K}_k is the Kalman gain.

In step-two, the lever arm error equation is formulated as follows:

$$\mathbf{v}_{\text{nhc}}^u + \delta \mathbf{v}_{\text{nhc}}^u = \hat{\mathbf{C}}_b^u \mathbf{C}_n^b \mathbf{v}_{\text{sins}}^n + \hat{\mathbf{C}}_b^u (\bar{\omega}_{nb}^b \times) (\delta \mathbf{l}^b) \quad (32)$$

and then the lever arm error equation is given by

$$\delta \mathbf{v}_{\text{nhc}}^u = \hat{\mathbf{C}}_b^u (\bar{\omega}_{nb}^b \times) (\delta \mathbf{l}^b) \quad (33)$$

where $\hat{\mathbf{C}}_b^u$ is the estimated mounting error angle, and $\bar{\omega}_{nb}$ denote the gyro angular rate of the posterior SINS/GNSS turn-driving data, and the measurement matrix \mathbf{H}_{la} is given by

$$\mathbf{H}_{\text{la},k} = [\hat{\mathbf{C}}_b^u (\bar{\omega}_{nb}^b \times)] \quad (34)$$

If the estimate of mounting error angle is assumed to be relatively accurate, the lever arm error measurement equation in (33) can be further formulated as

$$\begin{aligned} \delta \mathbf{v}_{\text{nhc},x}^b &= -\bar{\omega}_{nb}^z \delta l_y^b + \bar{\omega}_{nb}^y \delta l_z^b \approx -\bar{\omega}_{nb}^z \delta l_y^b \\ \delta \mathbf{v}_{\text{nhc},z}^b &= -\bar{\omega}_{nb}^y \delta l_x^b + \bar{\omega}_{nb}^x \delta l_y^b \approx \bar{\omega}_{nb}^x \delta l_y^b \end{aligned} \quad (35)$$

where it indicates that the forward lever arm has the greatest influence on the NHC [30]. In addition, the lever arm is assumed the constant value, and the corresponding state error variable and state matrix are formulated as follows, respectively

$$\mathbf{x}_{\text{la}} = [\delta \mathbf{l}^b]^T, \mathbf{F}_{\text{la},k|k-1} = \mathbf{I}_3 \quad (36)$$

and the corresponding SSM is formulated as follows.

$$\begin{aligned} \mathbf{x}_{\text{la},k|k-1} &= \mathbf{F}_{\text{la},k|k-1} \mathbf{x}_{\text{la},k-1} + \boldsymbol{\sigma}_{\text{la}} \\ \mathbf{z}_{\text{la},k} &= \mathbf{H}_{\text{la},k} \mathbf{x}_{\text{la},k|k-1} + \boldsymbol{\nu}_{\text{la}} \end{aligned} \quad (37)$$

where $\boldsymbol{\sigma}_{\text{la}}$ and $\boldsymbol{\nu}_{\text{la}}$ denote the Gaussian noise, i.e., $\boldsymbol{\sigma}_{\text{la}} \sim \mathcal{N}(\mathbf{0}, \mathbf{Q}_{\text{la}})$ and $\boldsymbol{\nu}_{\text{la}} \sim \mathcal{N}(\mathbf{0}, \mathbf{R}_{\text{la}})$. In addition, the measurement innovation $\mathbf{z}_{\text{la},k}$ can be obtained by (9). Consequently, based on state equation in (36) and measurement equation in (33), the lever arm of NHC can be easily estimated by KF framework. Correspondingly the time update and measurement update are formulated as follows.

c) Time update:

$$\begin{aligned} \mathbf{x}_{\text{la},k|k-1} &= \mathbf{F}_{\text{la},k|k-1} \mathbf{x}_{\text{la},k-1} \\ \mathbf{P}_{k|k-1} &= \mathbf{F}_{\text{la},k|k-1} \mathbf{P}_{k-1} (\mathbf{F}_{\text{la},k|k-1})^T + \mathbf{Q}_{\text{la},k-1} \end{aligned} \quad (38)$$

Algorithm 1: The estimation of mounting error angle and lever arm (RIEKF-based VDR method)

Inputs: $\hat{\mathbf{x}}_{\text{ma},k-1}^R, \mathbf{P}_{\text{ma},k-1}^R, \Phi_{k|k-1}^R, \Gamma_{k-1}^R, \mathbf{H}_{\text{ma}}^R, \mathbf{d}\mathbf{z}_{\text{ma},k}^R, \mathbf{Q}_{\text{ma}}$, $\mathbf{R}_{\text{ma}}, [\mathbf{C}_b^n, \mathbf{v}_{eb}^n, \mathbf{r}_{eb}^n] \{\text{posterior}\}, \mathbf{r}_{\text{vdr},k-1}^n, \Delta \mathbf{s}_k^u, \mathbf{C}_b^u, \delta \mathbf{l}^b$

VDR update:

1. Update VDR position based on the straight-driving data

$$\mathbf{r}_{\text{vdr},k}^n = \mathbf{r}_{\text{vdr},k-1}^n + \mathbf{C}_b^n \mathbf{C}_u^b \Delta \mathbf{s}_k^u$$

Step-one: mounting error angle estimation:

Time update:

2. Calculate the $\hat{\mathbf{x}}_{\text{ma},k|k-1}^R$ and $\mathbf{P}_{\text{ma},k|k-1}^R$

$$\hat{\mathbf{x}}_{\text{ma},k|k-1}^R = \Phi_{k|k-1}^R \hat{\mathbf{x}}_{\text{ma},k-1}^R$$

$$\mathbf{P}_{\text{ma},k|k-1}^R = \Phi_{k|k-1}^R \mathbf{P}_{\text{ma},k-1}^R (\Phi_{k|k-1}^R)^T + \Gamma_{k-1}^R \mathbf{Q}_{\text{ma}} (\Gamma_{k-1}^R)^T$$

Measurement update:

3. Calculate the $\hat{\mathbf{x}}_{\text{ma},k}^R$ and $\hat{\mathbf{P}}_{\text{ma},k}^R$

$$\mathbf{K}_k = \mathbf{P}_{\text{ma},k|k-1}^R (\mathbf{H}_{\text{ma}}^R)^T \left[\mathbf{H}_{\text{ma}}^R \mathbf{P}_{\text{ma},k|k-1}^R (\mathbf{H}_{\text{ma}}^R)^T + \mathbf{R}_{\text{ma}} \right]^{-1}$$

$$\hat{\mathbf{x}}_{\text{ma},k}^R = \hat{\mathbf{x}}_{\text{ma},k|k-1}^R + \mathbf{K}_k [\mathbf{d}\mathbf{z}_{\text{ma},k}^R - \mathbf{H}_{\text{ma}}^R \hat{\mathbf{x}}_{\text{ma},k|k-1}^R]$$

$$\hat{\mathbf{P}}_{\text{ma},k}^R = \mathbf{P}_{\text{ma},k|k-1}^R - \mathbf{K}_k \mathbf{H}_{\text{ma}}^R \mathbf{P}_{\text{ma},k|k-1}^R$$

Based on the posterior state $\hat{\mathbf{x}}_{\text{ma},k}^R$, the mounting error angle can be compensated accordingly.

Step-two: lever arm estimation:

4. Using turn-driving data and estimated mounting error angle, the SSM is constructed in (34), (36), and (37). Then, the lever arm will be easily estimated by (38) and (39).

Outputs: $\hat{\mathbf{C}}_b^u, \delta \mathbf{l}^b$

d) Measurement update:

$$\begin{aligned} \mathbf{K}_k &= \mathbf{P}_{k|k-1} (\mathbf{H}_{\text{la},k})^T \left(\mathbf{H}_{\text{la},k} \mathbf{P}_{k|k-1} (\mathbf{H}_{\text{la},k})^T + \mathbf{R}_{\text{la},k} \right)^{-1} \\ \mathbf{x}_{\text{la},k|k} &= \mathbf{x}_{\text{la},k|k-1} + \mathbf{K}_k (\mathbf{z}_{\text{la},k} - \mathbf{H}_{\text{la},k} \mathbf{x}_{\text{la},k|k-1}) \\ \mathbf{P}_{k|k} &= (\mathbf{I}_3 - \mathbf{K}_k \mathbf{H}_{\text{la},k}) \mathbf{P}_{k|k-1} \end{aligned} \quad (39)$$

where $\mathbf{Q}_{\text{la},k-1}$ and $\mathbf{R}_{\text{la},k}$ denote the corresponding the state noise covariance matrix and measurement noise covariance matrix, respectively. In order to better demonstrate the proposed method, the corresponding algorithm pseudo-code is given in Algorithm 1.

V. PROPOSED IMPROVED GSTM-BASED VB ROBUST FILTERING FOR INTERMITTENT GNSS OUTAGE

A. LG-based NHC state space model

In the autonomous vehicle navigation, the state update equation of SINS satisfying group affine system are given as follows [31]

$$\begin{aligned} \dot{\mathbf{C}}_b^u &= \mathbf{C}_b^n (\bar{\omega}_{nb}^b \times) - (\bar{\omega}_{in}^n \times) \mathbf{C}_b^n \\ \dot{\mathbf{v}}_{ib}^n &= -(\bar{\omega}_{in}^n \times) \mathbf{v}_{ib}^n + \mathbf{C}_b^n \mathbf{f}_{ib}^b + \mathbf{G}^n \\ \dot{\mathbf{r}}_{ib}^n &= -(\bar{\omega}_{in}^n \times) \mathbf{r}_{ib}^n + \mathbf{v}_{ib}^n \end{aligned} \quad (40)$$

where \mathbf{G}^n denotes the gravitational force projected to n frame, and the relationship between gravitational force \mathbf{G}^n and gravity \mathbf{g}^n is as follows

$$\mathbf{G}^n = \mathbf{g}^n + (\bar{\omega}_{ie}^n \times)^2 \mathbf{r}_{ib}^n \quad (41)$$

The gyroscope output models are given by

$$\begin{aligned} \bar{\omega}_{ib}^b &= \tilde{\omega}_{ib}^b - \varepsilon^b - \mathbf{w}_{\text{gyro}} \\ \varepsilon^b &= \mathbf{0} \end{aligned} \quad (42)$$

where $\tilde{\omega}_{ib}^b$ denotes the error contaminated angular rate, ε^b is constant bias, and \mathbf{w}_{gyro} is zero-mean Gaussian white noise.

Similarly, the accelerometer output models are given by

$$\begin{aligned} \mathbf{f}^b &= \tilde{\mathbf{f}}^b - \nabla^b - \mathbf{w}_{\text{acc}} \\ \dot{\nabla}^b &= \mathbf{0} \end{aligned} \quad (43)$$

where $\tilde{\mathbf{f}}^b$ denotes the error contaminated specific force, ∇^b is constant bias, and \mathbf{w}_{acc} is zero-mean Gaussian white noise. Furthermore, the left invariant error is defined as

$$\mathbf{x}_{\text{nav}}^L = [\phi_{\text{nav}}^b \ \zeta_v^L \ \zeta_r^L \ \varepsilon_b \ \nabla_b]^T \quad (44)$$

where ϕ_{nav}^b , ζ_v^L , and ζ_r^L denote left invariant error state of the misalignment angle, velocity, and position, respectively, and the corresponding left invariant error-based state equation is given by

$$\mathbf{x}_{\text{nav},k|k-1}^L = \mathbf{F}_{k|k-1}^L \mathbf{x}_{\text{nav},k-1}^L + \mathbf{G}_{k|k-1}^L \mathbf{w}_b \quad (45)$$

where \mathbf{w}_b is assumed to be Gaussian distribution, i.e., $\mathbf{w}_b \sim N(\mathbf{0}, \mathbf{Q}_k)$ and $\mathbf{w}_b = [\mathbf{w}_{\text{gyro}}, \mathbf{w}_{\text{acc}}]^T$, and

$$\mathbf{F}_{k|k-1}^L = \begin{bmatrix} \mathbf{F}_i^L & \mathbf{F}_s^L \\ \mathbf{0}_{6 \times 9} & \mathbf{0}_{6 \times 6} \end{bmatrix}, \mathbf{G}_{k|k-1}^L = \begin{bmatrix} -\mathbf{I}_6 \\ \mathbf{0}_{9 \times 6} \end{bmatrix} \quad (46)$$

and

$$\mathbf{F}_i^L = \begin{bmatrix} -\tilde{\omega}_{ib}^b \times & \mathbf{0}_3 & \mathbf{0}_3 \\ -\tilde{\mathbf{r}}_{ib}^b \times & -\tilde{\omega}_{ib}^b \times & \mathbf{0}_3 \\ \mathbf{0}_3 & \mathbf{I}_3 & -\tilde{\omega}_{ib}^b \times \end{bmatrix} \mathbf{F}_s^L = \begin{bmatrix} -\mathbf{I}_6 \\ \mathbf{0}_{3 \times 6} \end{bmatrix} \quad (47)$$

Remark 2. Actually, according to the definition of invariant error, there are also two state error models, which exist respectively in LIEKF and RIEKF. However, as compared with state error equation model of RIEKF, the state error equation model of LIEKF has better state independence, so it is not affected by navigation state uncertainty. Since the time update frequency is much higher than the measurement update frequency, the state independence of the state error equation model is particularly important in low-accuracy MEMS-bases SINS navigation. Moreover, the LIEKF has a natural advantage in dealing with intermittent GNSS outage, and this advantage is also due to its strong state independence. In other words, the LIEKF can maintain a good estimation consistency during the intermittent GNSS outage, so that the estimation accuracy of navigation state can still be maintained within a certain range. Accordingly, we can also conclude that the left invariant error-based NHC measurement model has good state independence. The detailed derivation process and analyses are given in the following Section V. B.

B. Proposed Novel LG-based NHC measurement model

In order to improve the estimation consistency of the existing NHC method, the left invariant error-based NHC measurement equation is proposed, and its core is to build the mathematical relationship between the NHC measurement innovation and the invariant error. Meanwhile, since the mounting error angle and lever arm are accurately estimated during the off-line calibration stage, they are maintained as constant values throughout the process. In **Theorem 2** and its proof, the left invariant error-based NHC measurement model and its derivation are given, respectively.

Theorem 2. Based on the estimated mounting error angle and lever arm, the proposed novel left invariant error-based NHC measurement equation is defined as follows

$$\mathbf{z}_{\text{nhc},k}^L = \mathbf{H}_{\text{nhc}}^L \mathbf{x}_{\text{nav},k|k-1}^L + \boldsymbol{\nu}_{\text{nhc}}^L \quad (48)$$

where $\mathbf{z}_{\text{nhc}}^L$ and $\boldsymbol{\nu}_{\text{nhc}}^L$ denote the measurement innovation and measurement noise, respectively. In addition, the measurement matrix $\mathbf{H}_{\text{nhc}}^L$ is formulated as follows

$$\mathbf{H}_{\text{nhc}}^L = \begin{bmatrix} \mathbf{h}_{\{1,1\}}^L & \mathbf{h}_{\{1,2\}}^L & \mathbf{h}_{\{1,3\}}^L & \mathbf{h}_{\{1,4\}}^L & \mathbf{0}_{1 \times 3} \\ \mathbf{h}_{\{2,1\}}^L & \mathbf{h}_{\{2,2\}}^L & \mathbf{h}_{\{2,3\}}^L & \mathbf{h}_{\{2,4\}}^L & \mathbf{0}_{1 \times 3} \end{bmatrix} \quad (49)$$

where

$$\begin{cases} \mathbf{h}_{\{1,1\}}^L = -\hat{\mathbf{C}}_b^u (\mathbf{v}_{\text{sins}}^b) \times (1,:) \\ \mathbf{h}_{\{1,2\}}^L = -\hat{\mathbf{C}}_b^u (1,:) \\ \mathbf{h}_{\{1,3\}}^L = \hat{\mathbf{C}}_b^u (\mathbf{C}_n^b \boldsymbol{\omega}_{ie}^n) \times (1,:) \\ \mathbf{h}_{\{1,4\}}^L = -\hat{\mathbf{C}}_b^u (\hat{\mathbf{l}}^b \times) (1,:) \end{cases} \quad (50)$$

and

$$\begin{cases} \mathbf{h}_{\{2,1\}}^L = -\hat{\mathbf{C}}_b^u (\mathbf{v}_{\text{sins}}^b) \times (3,:) \\ \mathbf{h}_{\{2,2\}}^L = -\hat{\mathbf{C}}_b^u (3,:) \\ \mathbf{h}_{\{2,3\}}^L = \hat{\mathbf{C}}_b^u (\mathbf{C}_n^b \boldsymbol{\omega}_{ie}^n) \times (3,:) \\ \mathbf{h}_{\{2,4\}}^L = -\hat{\mathbf{C}}_b^u (\hat{\mathbf{l}}^b \times) (3,:) \end{cases} \quad (51)$$

where $\hat{\mathbf{C}}_b^u$ and $\hat{\mathbf{l}}^b$ denote the estimated mounting error angle matrix and lever arm, respectively. The estimated $\hat{\mathbf{C}}_b^u$ and $\hat{\mathbf{l}}^b$ are obtained from off-line calibration in Section IV and are considered as constant variables throughout the entire navigation estimation process.

Proof: See Appendix C. ■

Remark 3. Compared to the existing NHC model in (11)-(13), the proposed left invariant error-based NHC measurement model exhibits better state independence. Specifically, $\mathbf{h}_{\{1,2\}}^L$ and $\mathbf{h}_{\{2,2\}}^L$ are considered as constant variables, whereas in existing NHC method, both are related to the attitude matrix \mathbf{C}_n^b . Hence, when there is an error in the estimated attitude \mathbf{C}_n^b , the proposed left invariant error-based NHC measurement model can still demonstrate better consistency to some extent. Moreover, although the proposed left invariant error-based NHC measurement model incorporates the attitude matrix \mathbf{C}_n^b in $\mathbf{h}_{\{1,3\}}^L$ and $\mathbf{h}_{\{2,3\}}^L$, it is coupled with the angular rate $\boldsymbol{\omega}_{ie}^n$. Since the $\boldsymbol{\omega}_{ie}^n$ is very small in the low-speed autonomous vehicles navigation, the impact of $\mathbf{C}_n^b \boldsymbol{\omega}_{ie}^n$ on the measurement model will also be very minimal. Actually, based on the definition of right invariant error, the right invariant error-based NHC measurement model can also be obtained. However, through our detailed analyses, it can be concluded that the state independence of right invariant error-based NHC measurement model is worse than that of the proposed left invariant error-based NHC measurement model. Therefore, in this paper, we mainly focus on the proposed left invariant error-based NHC method, while the less effective right invariant error-based NHC method is only used as a comparative reference.

C. Proposed improved GSTM-based VB robust filtering for intermittent GNSS outage

For the actual complex road environment of autonomous vehicles, the improved GSTM-based VB robust filtering is proposed. Aiming at the noise characteristics, firstly, it is modeled as GSTM distribution to improve the robustness. Then, a strong tracking strategy is used to fine-calibrate the initial nominal measurement covariance matrix to further enhance the response to uncertainty noise. Finally, the iterative joint estimation of states and parameters is realized in the VB framework.

1) GSTM-based robust filtering in the VB framework:

The probability density function of the GSTM distributed random vector \mathbf{x} conditioned on the mixing probability π_k is formulated as follows [36]

$$p(\mathbf{x}_k | \pi_k) = \pi_k N(\mathbf{x}_k; \boldsymbol{\mu}_k, \boldsymbol{\Sigma}_k) + (1 - \pi_k) St(\mathbf{x}_k; \boldsymbol{\mu}_k, \boldsymbol{\Sigma}_k, v_k) \quad (52)$$

where $\boldsymbol{\mu}_k$, $\boldsymbol{\Sigma}_k$, v_k , and π_k denote the mean, scale matrix, dof parameter, and the mixing probability, respectively. In addition, by introducing a Bernoulli random variable y_k , the hierarchical Gaussian forms of (52) can be formulated as follows [36]

$$\begin{aligned} p(\mathbf{z}_k | \mathbf{x}_k, \lambda_k, y_k) &= [N(\mathbf{z}_k; \mathbf{H}_k \mathbf{x}_{k|k-1}, \mathbf{R}_k)]^{y_k} \\ &\times [N(\mathbf{z}_k; \mathbf{H}_k \mathbf{x}_{k|k-1}, \mathbf{R}_k / \lambda_k)]^{1-y_k} \quad \text{s.t. } y_k \in \{0, 1\} \end{aligned} \quad (53)$$

and

$$p(\lambda_k) = G(\lambda_k; \frac{v_k}{2}, \frac{v_k}{2}) \quad (54)$$

where \mathbf{R}_k and λ_k denotes the initial nominal measurement covariance matrix and auxiliary variable, respectively.

Further, based on the VB framework, the latent variables $\Xi_k = \{\mathbf{x}_k, \lambda_k, y_k, \pi_k\}$ are jointly estimated, where the $\hat{\mathbf{x}}_{k|k}^{(i+1)}$ and $\mathbf{P}_{k|k}^{(i+1)}$ are calculated iteratively as follows [41]

$$\begin{cases} \mathbf{K}_k^{(i+1)} = \mathbf{P}_{k|k-1} \mathbf{H}_k^T (\mathbf{H}_k \mathbf{P}_{k|k-1} \mathbf{H}_k^T + \hat{\mathbf{R}}_k^{(i+1)})^{-1} \\ \hat{\mathbf{x}}_{k|k}^{(i+1)} = \hat{\mathbf{x}}_{k|k-1} + \mathbf{K}_k^{(i+1)} (\mathbf{z}_k - \mathbf{H}_k \hat{\mathbf{x}}_{k|k-1}) \\ \mathbf{P}_{k|k}^{(i+1)} = \mathbf{P}_{k|k-1} - \mathbf{K}_k^{(i+1)} \mathbf{H}_k \mathbf{P}_{k|k-1} \end{cases} \quad (55)$$

and $\hat{\mathbf{x}}_{k|k-1}$ and $\mathbf{P}_{k|k-1}$ are formulated as follows:

$$\begin{aligned} \hat{\mathbf{x}}_{k|k-1} &= \mathbf{F}_{k|k-1} \hat{\mathbf{x}}_{k-1|k-1} \\ \mathbf{P}_{k|k-1} &= \mathbf{F}_{k|k-1} \mathbf{P}_{k-1|k-1} \mathbf{F}_{k|k-1}^T + \mathbf{G}_{k-1} \mathbf{Q}_{k-1} \mathbf{G}_{k-1}^T \end{aligned} \quad (56)$$

where the modified $\hat{\mathbf{R}}_k^{(i+1)}$ is given by:

$$\hat{\mathbf{R}}_k^{(i+1)} = \frac{\mathbf{R}_k}{E^{(i+1)}[y_k] + (1 - E^{(i+1)}[y_k])E^{(i+1)}[\lambda_k]} \quad (57)$$

where the y_k is updated as the Bernoulli distribution, and $E^{(i+1)}[y_k]$ is formulated as [36]

$$E^{(i+1)}[y_k] = \frac{Pr_{y_k=1}^{(i+1)}}{Pr_{y_k=1}^{(i+1)} + Pr_{y_k=0}^{(i+1)}} \quad (58)$$

where

$$\begin{aligned} Pr_{y_k=1}^{(i+1)} &= \Delta^{(i+1)} \exp\{E^{(i)}[\log(\pi_k)] - 0.5 \text{tr}(\mathbf{B}_k^{(i+1)} \mathbf{R}_k^{-1})\} \\ Pr_{y_k=0}^{(i+1)} &= \Delta^{(i+1)} \exp\{E^{(i)}[\log(1 - \pi_k)] + 0.5 n_z E^{(i)}[\log \lambda_k] \\ &\quad - 0.5 E^{(i)}[\lambda_k] \text{tr}(\mathbf{B}_k^{(i+1)} \mathbf{R}_k^{-1})\} \end{aligned} \quad (59)$$

where $\Delta^{(i+1)}$ denotes the normalizing constant, and n_z denotes the dimension of measurement vectors, and the auxiliary parameter $\mathbf{B}_k^{(i+1)}$ is formulated as follows

$$\mathbf{B}_k^{(i+1)} = (\mathbf{z}_k - \mathbf{H}_k \hat{\mathbf{x}}_{k|k}^{(i+1)})(\mathbf{z}_k - \mathbf{H}_k \hat{\mathbf{x}}_{k|k}^{(i+1)})^T + \mathbf{H}_k \mathbf{P}_{k|k}^{(i+1)} \mathbf{H}_k^T \quad (60)$$

In addition, π_k is update as Beta distribution, the $E^{(i+1)}[\log(\pi_k)]$ and $E^{(i+1)}[\log(1 - \pi_k)]$ are, respectively, formulated as [36]

$$\begin{cases} E^{(i+1)}[\log(\pi_k)] = \psi(e_k^{(i+1)}) - \psi(e_k^{(i+1)} + f_k^{(i+1)}) \\ E^{(i+1)}[\log(1 - \pi_k)] = \psi(f_k^{(i+1)}) - \psi(e_k^{(i+1)} + f_k^{(i+1)}) \end{cases} \quad (61)$$

where $\psi(\cdot)$ is the logarithmic derivative of the gamma function, and then the shape parameters $e_k^{(i+1)}$ and $f_k^{(i+1)}$ are, respectively, formulated as follows:

$$\begin{cases} e_k^{(i+1)} = e_0 + E^{(i+1)}[y_k] \\ f_k^{(i+1)} = 2 - e_0 - E^{(i+1)}[y_k] \end{cases} \quad (62)$$

In addition, λ_k is update as Gamma distribution, and then the $E^{(i+1)}[\lambda_k]$ and $E^{(i+1)}[\log(\lambda_k)]$ are, respectively, formulated as follows [36]

$$\begin{cases} E^{(i+1)}[\lambda_k] = \frac{\xi_k^{(i+1)}}{\varsigma_k^{(i+1)}} \\ E^{(i+1)}[\log(\lambda_k)] = \psi(\xi_k^{(i+1)}) - \log(\varsigma_k^{(i+1)}) \end{cases} \quad (63)$$

where the shape $\xi_k^{(i+1)}$ and rate parameter $\varsigma_k^{(i+1)}$ are, respectively, formulated as follows:

$$\begin{cases} \xi_k^{(i+1)} = 0.5(n_z(1 - E^{(i+1)}[y_k]) + v_k) \\ \varsigma_k^{(i+1)} = 0.5(\text{tr}(\mathbf{B}_k^{(i+1)} \mathbf{R}_k^{-1})(1 - E^{(i+1)}[y_k]) + v_k) \end{cases} \quad (64)$$

2) Strong tracking-based nominal measurement covariance matrix correction:

In theory, the innovation covariance matrix \mathbf{C}_k approximates as follows [42]

$$\mathbf{C}_k \approx \mathbf{N}_k + \mathbf{R}_k \quad (65)$$

where \mathbf{N}_k and \mathbf{C}_k can be, respectively, calculated as follows

$$\mathbf{N}_k = \mathbf{H}_k (\mathbf{F}_{k|k-1} \mathbf{P}_{k-1} \mathbf{F}_{k|k-1}^T + \mathbf{G}_{k-1} \mathbf{Q}_{k-1} \mathbf{G}_{k-1}^T) \mathbf{H}_k^T \quad (66)$$

$$\mathbf{C}_k = (1 - \epsilon_k) \mathbf{C}_{k-1} + \epsilon_k (\mathbf{z}_k \mathbf{z}_k^T) \quad (67)$$

and

$$\epsilon_k = \frac{\epsilon_{k-1}}{\epsilon_{k-1} + b} \quad (68)$$

where $\epsilon_0 = 1$ and $b \in [0.9, 0.999]$ denotes the fading factor. However, in actual systems, the uncertainty outlier noise will be introduced into the innovation covariance matrix, thus leading to a severe mismatch in (65). In order to mitigate the effects of innovation mismatch, the strong tracking method is introduced. The core of this method is to dynamically adjust the initial nominal covariance matrix by using a proportional coefficient, so as to compensate the mismatch of the innovation matrix to a certain extent. By introducing the proportional coefficient κ_k , (65) can be reformulated as follows:

$$\mathbf{C}_k - \mathbf{N}_k = \kappa_k \mathbf{R}_k \quad (69)$$

Algorithm 2: The IGSTM-based VB robust filtering for intermittent GNSS outage (proposed IGSTM-LIEKF).

Inputs: $\mathbf{x}_{\text{nav},k-1}^L$, \mathbf{P}_{k-1} , $\mathbf{F}_{k|k-1}^L$, $\mathbf{G}_{k|k-1}^L$, $\mathbf{H}_{\text{nnc}}^L$, $\mathbf{z}_{\text{nnc}}^L$, \mathbf{Q}_{k-1} , $\mathbf{R}_{\text{nnc}}, N_m, n_z, \hat{\mathbf{C}}_b^u, \hat{\mathbf{b}}^b, \mathbf{X}_k = \{\mathbf{C}_b^n, \mathbf{v}_{ib}^n, \mathbf{r}_{ib}^n\}, \mathbf{b}_k = \{\boldsymbol{\epsilon}, \nabla_b\}, e_0, f_0, b, \epsilon_0, \mathbf{C}_{k-1}, v_k$

SINS state update: 1. Update the SINS state using (40).

Time update: 2. Calculate the $\hat{\mathbf{x}}_{\text{nav},k|k-1}^L$ and $\mathbf{P}_{k|k-1}$ using (56).

Improved GSTM-based measurement update:

3. Initialization: $\hat{\mathbf{x}}_{\text{nav},0}^L = \mathbf{x}_{k|k-1}$, $E[\log(\lambda_0)] = 0, \epsilon_0 = 1$

$E[\log(\pi_0)] = \psi(e_0) - \psi(1), E[\lambda_0] = 1, b = 0.9, v_k = 3$

$E[\log(1 - \pi_0)] = \psi(1 - e_0) - \psi(1), E[y_0] = 1$

$\hat{\mathbf{C}}_{k-1} = 10\mathbf{R}_{\text{nnc},k}, e_0 = 0.85, f_0 = 0.15$

4. Fine-calibrate the initial nominal measurement covariance matrix $\bar{\mathbf{R}}_k$ using (66)-(71).

for $i = 0 : N_m - 1$

5. Calculate the modified $\hat{\mathbf{R}}_k^{(i+1)}$ using (57), and calculate $\hat{\mathbf{x}}_{k|k}^{(i+1)}$ and $\mathbf{P}_{k|k}^{(i+1)}$ using (55).

7. Calculate $\Pr_{y_k=1}^{(i+1)}$ and $\Pr_{y_k=0}^{(i+1)}$ using (59), and calculate $E^{(i+1)}[y_k]$ using (58).

8. Calculate $e_k^{(i+1)}$ and $f_k^{(i+1)}$ using (62), and calculate $E^{(i+1)}[\log(\pi_k)]$ and $E^{(i+1)}[\log(1 - \pi_k)]$ using (61).

9. Calculate $\xi_k^{(i+1)}$ and $\varsigma_k^{(i+1)}$ using (64), and calculate $E^{(i+1)}[\lambda_k]$ and $E^{(i+1)}[\log(\lambda_k)]$ using (63)

end for

10. $\hat{\mathbf{x}}_{k|k} = \hat{\mathbf{x}}_{k|k}^{(i)}, \mathbf{P}_{k|k} = \mathbf{P}_{k|k}^{(i)}$

State error correction:

11. $\hat{\mathbf{X}}_k = \tilde{\mathbf{X}}_k \exp(\hat{\mathbf{x}}_{k|k}(1 : 9)), \hat{\mathbf{b}}_k = \tilde{\mathbf{b}}_k + \hat{\mathbf{x}}_{k|k}(10 : 15)$

where the proportional coefficient κ_k is defined as

$$\kappa_k = \frac{\text{tr}(\mathbf{C}_k - \mathbf{N}_k)}{\text{tr}(\mathbf{R}_k)} \quad (70)$$

Actually, although the GSTM-based VB robust filtering algorithm can estimate the modified measurement covariance matrix $\bar{\mathbf{R}}_k$, this process is still based on the initial nominal covariance matrix \mathbf{R}_k . Therefore, in the initial phase of measurement update, the fine calibration of the nominal measurement covariance matrix will significantly benefit the proposed GSTM-based VB robust filtering algorithm to adapt more sensitively to environmental changes. Based on the above analysis, the initial nominal measurement covariance $\bar{\mathbf{R}}_k$ can be replaced by:

$$\bar{\mathbf{R}}_k = \kappa_k \mathbf{R}_k \quad (71)$$

The proposed improved GSTM-based VB robust filtering is composed of Section V. A-C, and the corresponding pseudo-code is shown in algorithm 2.

VI. SIMULATION TEST

In this section, the simulation trajectory of autonomous vehicle is designed to verify the effectiveness of the proposed consistent-robust SINS/GNSS/NHC integrated navigation method. The setting of detailed trajectory segment is

TABLE I: Sensor parameters characteristics in the simulation.

Sensor	Constant drift	Random error
Gyroscope	50°/h	0.1°/√h
Accelerometer	5000ug	100ug/√Hz
GNSS position	0	1m

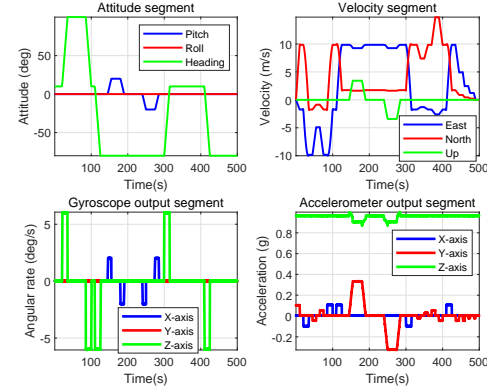


Fig. 6: Trajectory segment of the land-based vehicle simulation.

shown as Fig. 6, and the total time is 500s. The simulation actually include two parts. One part is to estimate mounting error angle and lever arm. The other part is to correct SINS navigation errors during intermittent GNSS outage. The parameters of gyroscope, accelerometer, and GNSS are listed in Table I. The output frequency of IMU and GNSS are set as 100Hz and 1Hz, respectively. For the proposed improved GSTM-based VB robust LIEKF (IGSTM-LIEKF), the EKF method, the R/LIEKF method, the NHC-EKF, the NHC-R/LIEKF, the GSTM-R/LIEKF, and the IGSTM-RIEKF are used as the comparison methods. In addition, the methods with the correction of mounting error angle and arm lever are marked with symbol $\{\triangle\}$. The initial errors of pitch, roll, and heading are set as 25°, 25° and 50°, respectively, and the initial velocity error and position error are set as 0.1m/s and 3m, respectively. In order to evaluate the estimation accuracy of different methods, the root-mean-square errors (RMSEs) and average root-mean-square errors (ARMSEs) are selected as performance indicators, and the RMSE and ARMSE are defined as follows.

$$\left\{ \begin{array}{l} \text{RMSE}_{\hat{\mathbf{x}}_k} \triangleq \sqrt{\frac{1}{N} \sum_{s=1}^N (\mathbf{x}_k^s - \hat{\mathbf{x}}_k^s)^2} \\ \text{ARMSE}_{\hat{\mathbf{x}}_k} \triangleq \sqrt{\frac{1}{NT} \sum_{k=1}^T \sum_{s=1}^N (\mathbf{x}_k^s - \hat{\mathbf{x}}_k^s)^2} \end{array} \right. \quad (72)$$

where \mathbf{x}_k^s and $\hat{\mathbf{x}}_k^s$ denote the true and estimated navigation state vectors at time k in the s -th Monte Carlo runs, respectively, and N and T denote the total Monte Carlo runs number and simulation time, respectively.

A. Proposed mounting error angle and lever arm estimate method

For the estimation of mounting error angle, the initial mounting error angle is set as $[\gamma, \beta] = [1.5^\circ, 0.5^\circ]$. The initial state of the existing EKF-based VDR, the LIEKF-based VDR, and the proposed RIEKF-based VDR are all set as $\mathbf{x}_{\text{ma},0} = \mathbf{0}_{8 \times 1}$. The state error covariance matrix $\mathbf{P}_{\text{ma},0}$ is set as $\text{diag}([0.3\text{m}\mathbf{I}_{3 \times 1}; 0.1^\circ\mathbf{I}_{2 \times 1}; 0.1^\circ\mathbf{I}_{3 \times 1}])^2$. In addition, the measurement noise covariance matrix $\mathbf{R}_{\text{ma},k}$ and state noise

covariance matrix $\mathbf{Q}_{ma,k}$ are set as $\text{diag}([0.15m\mathbf{I}_{3 \times 1}])^2$ and $\text{diag}([0.01^\circ/\sqrt{h}\mathbf{I}_{3 \times 1}; 0.1^\circ/\sqrt{h}\mathbf{I}_{2 \times 1}])^2$, respectively. In order to better reflect the accuracy and stability of the proposed method, the straight-driving intervals of the 50s-80s and 350s-380s are used to estimate the mounting error angle, respectively. The estimated results are shown in Fig. 7 and Table II. For the proposed RIEKF-based VDR method, its state-transition matrix $\Phi_{k|k-1}^R$ in (25) does not include the increment Δs^n , and the increment Δs^n is actually derived from $\mathbf{C}_b^n \mathbf{C}_u^b \Delta s_k^u$. Therefore, to a certain extent, the influence of \mathbf{C}_b^n and \mathbf{C}_u^b on the state-transition matrix of the proposed RIEKF-based VDR method is weakened. Moreover, the weakening of the state dependence improves the estimation consistency and makes the estimation of the mounting error angle more accurate.

TABLE II: The MEANs of mounting error angle.

Methods	Pitch [°]	Heading [°]	MEANs([*] + [◊])/2	
			pitch [°]	heading [°]
EKF-VDR	1.369*/1.398 [°]	0.345*/0.396 [°]	1.384	0.371
LIEKF-VDR	1.343*/1.339 [°]	0.376*/0.459 [°]	1.341	0.418
RIEKF-VDR	1.528*/1.484[°]	0.524*/0.532[°]	1.506	0.528

*: The mean in the 50s-80s interval.

◊: The mean in the 350s-380s interval

Based on the analysis in Section IV. B, the forward lever arm of NHC will significantly affect the lateral and vertical velocity of NHC, and it can be accurately estimated by simple maneuvers. Therefore, the forward lever arm is estimated in this paper. The initial forward lever arm is set as 1m, and the measurement noise covariance matrix $\mathbf{R}_{la,k}$ and state noise covariance matrix $\mathbf{Q}_{la,k}$ are set as $\text{diag}([0.03m/s\mathbf{I}_{2 \times 1}])^2$ and $\text{diag}([0.001m\mathbf{I}_{3 \times 1}])^2$, respectively, and the initial state error covariance matrix $\mathbf{P}_{la,0}$ is set as $\text{diag}([0.1m\mathbf{I}_{3 \times 1}])^2$. In Fig. 8 of the estimated forward lever arm, the time segment of T1, T2, and T3 indicate that the forward lever arm can rapidly converge to the true value when the pitch and heading of land-based vehicle and the corresponding X-axis and Z-axis angular rates change. Consequently, this conclusion directly prove the analysis in Section IV. B.

B. Comparisons and analyses of the proposed improved GSTM-based VB robust filtering

In order to verify the superiority of the proposed method, the segment is designed in Fig. 6, and the outage time are set as 130s-200s and 250s-350s, respectively. The measurement noise covariance matrix $\mathbf{R}_{nhc,k}$ is set as $\text{diag}([0.01m/s\mathbf{I}_{2 \times 1}])^2$, and the state noise covariance matrix is set as $\text{diag}([0.3^\circ/\sqrt{h}\mathbf{I}_{3 \times 1}; 50\mu g/\sqrt{Hz}\mathbf{I}_{3 \times 1}])^2$, and the initial state error variable $\mathbf{x}_{nhc,0}$ is set as $\mathbf{0}_{15 \times 1}$. For the IGSTM-RIEKF and proposed IGSTM-LIEKF, $b = 0.9$, $\mathbf{C}_{k-1} = 10\mathbf{R}_{nhc,k}$, $\epsilon_0 = 1$, $e_0 = 0.85$, $f_0 = 0.15$, $v_k = 3$, $E[\lambda_0] = E[y] = 1$, and $E[\log(\lambda_0)] = 0$. In addition, the initial state error covariance matrix \mathbf{P}_0 is set as $\text{diag}([5^\circ\mathbf{I}_{3 \times 1}; 0.1m/s\mathbf{I}_{3 \times 1}; 1m\mathbf{I}_{3 \times 1}; 15^\circ/h\mathbf{I}_{3 \times 1}; 2mg\mathbf{I}_{3 \times 1}])^2$,

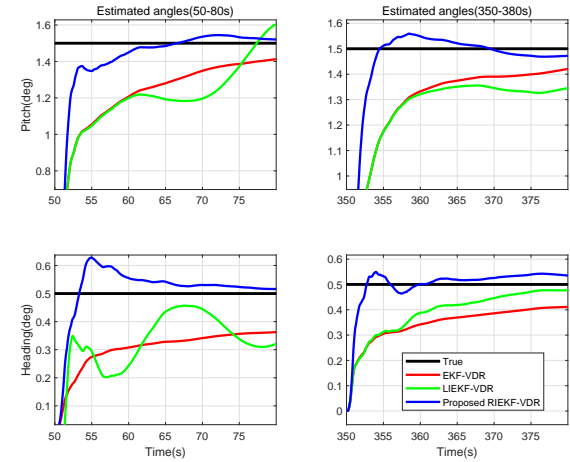


Fig. 7: Estimated mounting error angles in 50s-80s and 350s-380s.

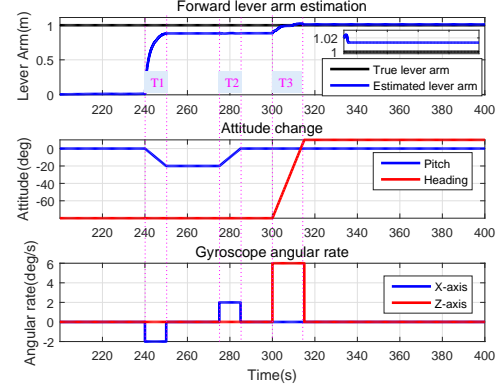


Fig. 8: Estimated forward lever arm of the land-based vehicle simulation.

and the initial state error covariance matrix \mathbf{P}_0^R and \mathbf{P}_0^L are, respectively, transformed as follows

$$\mathbf{P}_0^R = \boldsymbol{\Upsilon}^R \mathbf{P}_0 (\boldsymbol{\Upsilon}^R)^T \quad (73)$$

where

$$\boldsymbol{\Upsilon}^R = \begin{bmatrix} \mathbf{I}_3 & \mathbf{0}_3 & \mathbf{0}_3 & \mathbf{0}_3 & \mathbf{0}_3 \\ (\mathbf{v}_{ib}^n) \times & -\mathbf{I}_3 & (\mathbf{C}_{e0}^{n0} \boldsymbol{\omega}_{ie}) \times & \mathbf{0}_3 & \mathbf{0}_3 \\ (\mathbf{r}_{ib}^n) \times & \mathbf{0}_3 & -\mathbf{I}_3 & \mathbf{0}_3 & \mathbf{0}_3 \\ \mathbf{0}_3 & \mathbf{0}_3 & \mathbf{0}_3 & \mathbf{I}_3 & \mathbf{0}_3 \\ \mathbf{0}_3 & \mathbf{0}_3 & \mathbf{0}_3 & \mathbf{0}_3 & \mathbf{I}_3 \end{bmatrix} \quad (74)$$

and

$$\mathbf{P}_0^L = \boldsymbol{\Upsilon}^L \mathbf{P}_0 (\boldsymbol{\Upsilon}^L)^T \quad (75)$$

where

$$\boldsymbol{\Upsilon}^L = \begin{bmatrix} \mathbf{I}_3 & \mathbf{0}_3 & \mathbf{0}_3 & \mathbf{0}_3 & \mathbf{0}_3 \\ \mathbf{0}_3 & -\mathbf{C}_{n0}^{b0} & -\mathbf{C}_{n0}^{b0} (\mathbf{C}_{e0}^{n0} \boldsymbol{\omega}_{ie}) \times & \mathbf{0}_3 & \mathbf{0}_3 \\ \mathbf{0}_3 & \mathbf{0}_3 & -\mathbf{C}_{n0}^{b0} & \mathbf{0}_3 & \mathbf{0}_3 \\ \mathbf{0}_3 & \mathbf{0}_3 & \mathbf{0}_3 & \mathbf{I}_3 & \mathbf{0}_3 \\ \mathbf{0}_3 & \mathbf{0}_3 & \mathbf{0}_3 & \mathbf{0}_3 & \mathbf{I}_3 \end{bmatrix} \quad (76)$$

The NHC non-stationary outlier noise in the outage time

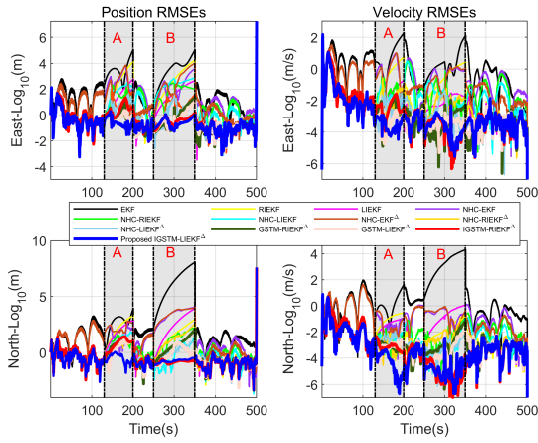


Fig. 9: Estimated position and velocity RMSEs of the land-based vehicle simulation.

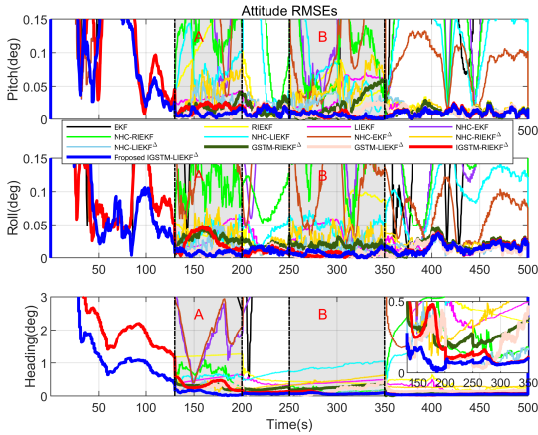


Fig. 10: Estimated attitude RMSEs of the land-based vehicle simulation.

interval [130s 200s] and [250s 350s] are generated as follows:

$$\left\{ \begin{array}{l} \nu_k \sim \begin{cases} N(0, (r_{nhc})^2) & \text{w.p. } p_1 \\ N(0, (50r_{nhc})^2) & \text{w.p. } 1 - p_1 \end{cases} \quad 130s \leq t_k < 150 \\ \nu_k \sim N(0, (r_{nhc})^2) \quad 150s \leq t_k < 170 \\ \nu_k \sim \begin{cases} N(0, (r_{nhc})^2) & \text{w.p. } p_2 \\ N(0, (30r_{nhc})^2) & \text{w.p. } 1 - p_2 \end{cases} \quad 170s \leq t_k \leq 200 \end{array} \right. \quad (77)$$

where $r_{nhc} = 0.1\text{m/s}$, and w.p. denotes “with probability”, and $p_1=0.9$ and $p_2=0.95$ denote the outlier probabilities, respectively.

$$\left\{ \begin{array}{l} \nu_k \sim N(0, (r_{nhc})^2) \quad 250s \leq t_k < 300 \\ \nu_k \sim \begin{cases} N(0, (r_{nhc})^2) & \text{w.p. } p_1 \\ N(0, (50r_{nhc})^2) & \text{w.p. } 1 - p_1 \end{cases} \quad 300s \leq t_k \leq 350 \end{array} \right. \quad (78)$$

The simulation results are shown in Fig. 9-10, and the outage time 130s-200s and 250s-350s are marked as the

“A” and “B”, respectively. The ARMSEs of the estimated navigation states in the GNSS outage time are listed in Table III-IV. In the RMSEs of position and velocity in Fig. 9, the logarithmic forms with base 10 of RMSEs are used to show the estimated results more clearly. Accordingly, the logarithmic forms with base 10 of position and velocity RMSEs in the east and north are abbreviated as the “East-log₁₀” and “North-log₁₀”, respectively. The results indicate that the estimation accuracy of the proposed IGSTM-LIEKF $^\Delta$ (blue line) is better than other methods during intermittent “Outage A” and “Outage B”. Meanwhile, the proposed IGSTM-LIEKF $^\Delta$ (blue line) is also superior to other methods in the attitude RMSEs of Fig. 10. In addition, in order to better demonstrate the advantages of the proposed method, the heading angle RMSEs in 130s-350s is locally amplified, and it indicates that the proposed method is superior to other methods in the case of intermittent GNSS outage. The main reason is that, on one hand, by estimating the mounting error angle and lever arm, the optimal performance framework of NHC can be achieved. In addition, in the proposed left invariant error-based NHC measurement model, the coefficient of velocity state error variable is constant, while in other methods, the coefficients of the velocity state error variables are related to the attitude matrix C_b^n . Consequently, the proposed left invariant error-based NHC measurement model has better estimation consistency. On the other hand, the GSTM distribution well models non-stationary outlier noise caused by the complex road environment. Meanwhile, by introducing strong tracking method, the initial NHC measurement covariance matrix is fine-calibrated to a certain extent, so as to better adapt to the change of uncertainty noise.

VII. CAR-MOUNTED FIELD TEST

The car-mounted field test is carried out to further verify the effectiveness of the proposed consistent-robust SIN-S/GNSS/NHC integrated navigation method. Since the primary objective of this paper is to propose a navigation method for intermittent GNSS outage, and due to the limitations of experimental conditions, we use a human-driven vehicle to conduct car-mounted field test. The platform is composed of SPAN-CPT [37], in which the gyroscope bias is about $20^\circ/\text{h}$ and the angle random walk is $0.0667^\circ/\sqrt{\text{h}}$. The accelerometer bias is 50mg, and bias stability is 0.75mg. In addition, the maximum output frequency of IMU and GNSS are 100Hz and 20Hz, respectively, and the GNSS positioning error is about 1m. The trajectory of the car-mounted field test and the moving segment are shown in Fig. 11 and Fig. 12, respectively, and 400s-600s and 600s-700s correspond to the curve-driving and the straight-driving, respectively. In Fig. 11, the red dashed line represents the artificially set GNSS outage interval.

In the car-mounted field test, the mounting error angle and lever arm of NHC should first be estimated to solve NHC mismatch. For the estimation of mounting error angle, the initial state covariance matrix of existing EKF-based method, the LIEKF-based method, and the proposed RIEKF-based method are all set as $\text{diag}([1\mathbf{I}_{3 \times 1}; 0.5^\circ \mathbf{I}_{2 \times 1}; [0.1^\circ, 0.1^\circ, 0.3^\circ];])^2$. And the measurement noise covariance matrix is set as

TABLE III: The ARMSEs of position and velocity in the 130s-350s simulation segment.

ARMSEs	EKF	R/LIEKF	NHC-EKF	NHC-RIEKF	NHC-LIEKF	GSTM-R/LIEKF	IGSTM-R/(proposed)LIEKF
East(m)	33.656	16.306/4.672	13.198/11.368 \triangle	5.372/2.069 \triangle	7.822/1.512 \triangle	0.936 \triangle / 0.771 \triangle	0.932 \triangle / 0.532 \triangle
North(m)	431.285	6.547/10.036	19.335/17.852 \triangle	2.795/2.619 \triangle	1.741/1.504 \triangle	1.746 \triangle /1.172 \triangle	1.052 \triangle / 0.508 \triangle
East(m/s)	2.104	0.622/0.146	0.839/0.683 \triangle	0.317/0.126 \triangle	0.275/0.084 \triangle	0.053 \triangle /0.036 \triangle	0.052 \triangle / 0.031 \triangle
North(m/s)	15.056	0.226/0.328	0.485/0.471 \triangle	0.115/0.091 \triangle	0.079/0.053 \triangle	0.054 \triangle /0.041 \triangle	0.026 \triangle / 0.015 \triangle

\triangle : With the correction of mounting error angle and lever arm.

TABLE IV: The attitude ARMSEs in the 130s-350s simulation segment.

ARMSEs	EKF	R/LIEKF	NHC-EKF	NHC-RIEKF	NHC-LIEKF	GSTM-R/LIEKF	IGSTM-R/(proposed)LIEKF
Pitch(deg)	1.811	0.072/0.031	0.328/0.245 \triangle	0.143/0.041 \triangle	0.095/0.025 \triangle	0.019 \triangle /0.011 \triangle	0.012 \triangle / 0.008 \triangle
Roll(deg)	1.840	0.039/0.031	0.268/0.185 \triangle	0.129/0.030 \triangle	0.039/0.017 \triangle	0.022 \triangle /0.007 \triangle	0.013 \triangle / 0.008 \triangle
Heading(deg)	12.479	0.695/0.445	3.862/4.241 \triangle	0.335/0.321 \triangle	0.735/0.218 \triangle	0.264 \triangle /0.192 \triangle	0.172 \triangle / 0.081 \triangle

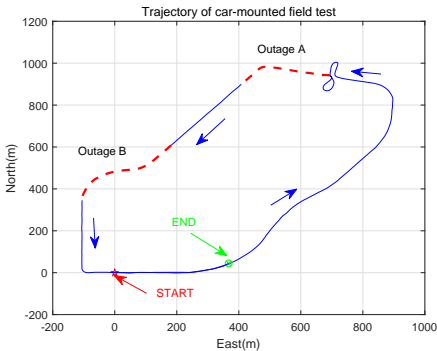


Fig. 11: Trajectory of the car-mounted field test.

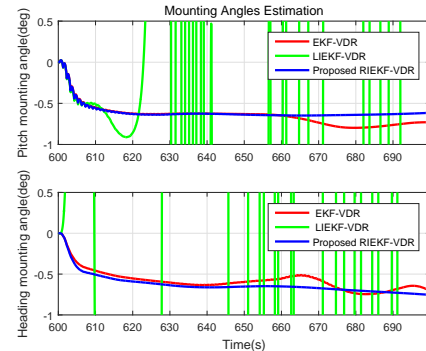


Fig. 13: Estimated mounting error angle of the car-mounted field test.

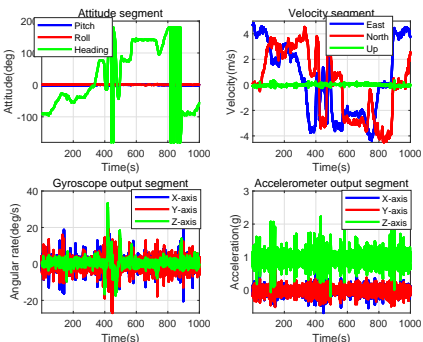


Fig. 12: Trajectory segment of the car-mounted field test.

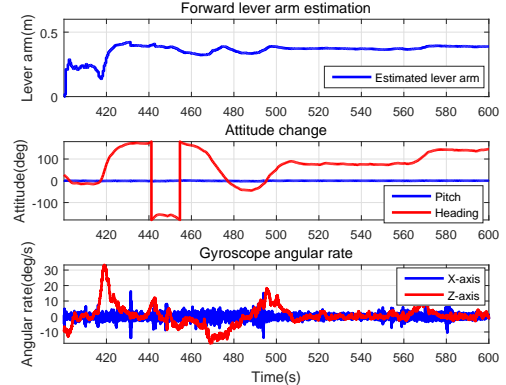


Fig. 14: Estimated lever arm of the car-mounted field test.

$\text{diag}([0.3\text{m}\mathbf{I}_{3 \times 1}])^2$, and the other initial parameters are set the same as Section VI. A. Fig. 13 indicates that the proposed RIEKF-based method has better stability than other methods, which is consistent with the conclusion in Section VI. A. However, the LIEKF-based VDR method shows serious divergence due to poor estimation consistency. For the estimation of NHC forward lever arm, the measurement noise covariance matrix $\mathbf{R}_{la,k}$ is set as $\text{diag}([0.1\text{m/s}\mathbf{I}_{2 \times 1}])^2$, and the other initial parameters are set the same as Section VI. A. Fig. 14 indicates that the forward lever arm can rapidly converge the fixed

value when the heading changes at 420s. Correspondingly, it shows that the observability of the estimated forward lever arm is greatly influenced by the Z-axis angular rate, and the conclusion is the same as in Section VI. A.

Based on the estimated mounting error angle and lever arm, the proposed IGSTM-based VB robust filtering for intermittent GNSS outage is further verified. In the proposed method, the measurement noise covariance matrix \mathbf{R}_k^{nhc} is

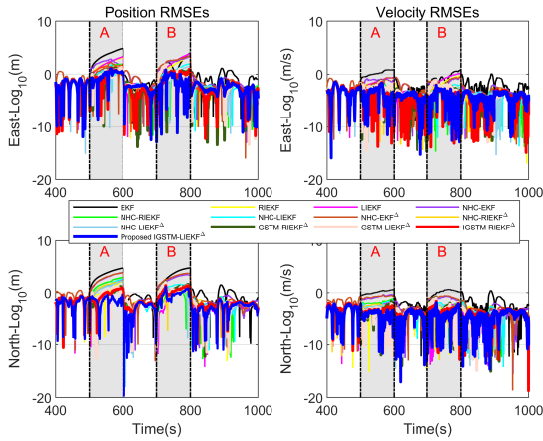


Fig. 15: Estimated horizontal position and velocity RMSEs of the car-mounted field test.

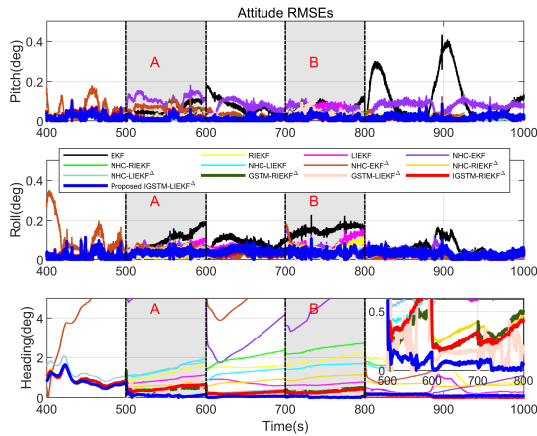


Fig. 16: Estimated attitude RMSEs of the car-mounted field test.

set as $\text{diag}([0.2\text{m}/\text{s}\mathbf{I}_{2 \times 1}])^2$, and the state noise covariance matrix is set as $\text{diag}([0.15^\circ/\sqrt{\text{h}}\mathbf{I}_{3 \times 1}; 100\mu\text{g}/\sqrt{\text{Hz}}\mathbf{I}_{3 \times 1}])^2$. Similarly with Section VI. B, the other parameters are set as $b=0.9$, $\mathbf{C}_{k-1} = 10\mathbf{R}_{\text{nhc},k}$, $\epsilon_0 = 1$, $e_0 = 0.85$, $f_0 = 0.15$, $v_k = 3$, $E[\lambda_0] = E[y] = 1$, and $E[\log(\lambda_0)] = 0$. In addition, the initial state error covariance matrix \mathbf{P}_0 is set as $\text{diag}([5^\circ\mathbf{I}_{3 \times 1}; 0.1\text{m}/\text{s}\mathbf{I}_{3 \times 1}; 1\text{m}\mathbf{I}_{3 \times 1}; 15^\circ/\text{h}\mathbf{I}_{3 \times 1}; 1\text{mg}\mathbf{I}_{3 \times 1}])^2$, and the corresponding initial state error covariance matrix \mathbf{P}_0^R and \mathbf{P}_0^L are obtained by (73) and (75), respectively.

Fig. 15-16 show the RMSEs of estimated navigation states, and the intermittent GNSS outage time 500s-600s and 700s-800s are marked as the “A” and “B”, respectively. However, in order to more clearly demonstrate the superiority of the proposed IGSTM-LIEKF $^\Delta$ (blue line) in intermittent GNSS outage, only the RMSEs of estimated navigation states in 400s-1000s are given. Similar to Section VI. B, the RMSEs of position and velocity in Fig. 15 are also represented as logarithmic forms. Then, in the intermittent GNSS “outage A” and “outage B”, it can be found that the proposed IGSTM-LIEKF $^\Delta$ (blue line) is better than other methods. Meanwhile, in the local magnification diagram of heading angle within 500s-800s in

Fig. 16, it can be found that the proposed IGSTM-LIEKF $^\Delta$ (blue line) still has great advantages during the intermittent GNSS outage, and the corresponding conclusions are the same as in Section VI.

VIII. CONCLUSION

In this paper, a consistent-robust SINS/GNSS/NHC integrated navigation method was proposed for autonomous vehicles under intermittent GNSS outage, which was divided into two stages. In the off-line calibration stage, the mounting error angle and lever arm are estimated to guarantee the best frame and effective point of NHC. In the online navigation stage, the more consistent NHC model is constructed. Then, the GSTM-based VB robust filtering is proposed to estimate the state and parameters under non-stationary outlier noise. In addition, the strong tracking method is introduced to further fine-calibrate the initial nominal measurement covariance matrix. Finally, the simulation and car-mounted field test results illustrate that the proposed consistent-robust method can effectively improve the navigation accuracy of autonomous vehicle during intermittent GNSS outage. As our further work, we will design a matching-based integrated navigation algorithm that uses road feature information to assist SINS, aimed at enhancing the navigation and positioning capability of the autonomous vehicles in the event of external auxiliary sensor failures.

REFERENCES

- [1] L. Chen et al., “Milestones in autonomous driving and intelligent vehicles: Survey of surveys”, *IEEE Transactions on intelligent vehicles.*, vol. 8, no. 2, pp. 1046-1056, Feb. 2023.
- [2] B. Paden, M. Čáp, S. Z. Yong, D. Yershov, and E. Frazzoli, “A survey of motion planning and control techniques for self-driving urban vehicles,” *IEEE Transactions on intelligent vehicles.*, vol. 1, no. 1, pp. 33-55, Mar. 2016.
- [3] S. Teng et al., “Motion planning for autonomous driving: The state of the art and future perspectives,” *IEEE Transactions on intelligent vehicles.*, vol. 8, no. 6, pp. 3692-3711, Jun. 2023.
- [4] S. Kuutti, S. Fallah, K. Katsaros, M. Dianati, F. McCullough, and A. Mouzakitis, “A survey of the state-of-the-art localization techniques and their potentials for autonomous vehicle applications,” *IEEE Internet Things J.*, vol. 5, no. 2, pp. 829-846, Apr. 2018.
- [5] G. Zhang, W. Wen, B. Xu, and L.-T. Hsu, “Extending shadow matching to tightly-coupled GNSS/INS integration system,” *IEEE Transactions on Vehicular Technology*, vol. 69, no. 5, pp. 4979-4991, May. 2020.
- [6] H. A. Ignatious, H.-E. Sayed, and M. Khan, “An overview of sensors in autonomous vehicles,” *Procedia Computer Science.*, vol. 198, pp. 736-741, Jan. 2022.
- [7] F. M. Ortiz, M. Sammarco, L. H. M. Costa, and M. Detyniecki, “Applications and services using vehicular exteroceptive sensors: A survey,” *IEEE Transactions on Intelligent Vehicles.*, vol. 8, no. 1, pp. 949-969, Jan. 2023.
- [8] J. Wahlström, I. Skog, P. Hänel, and A. Nehorai, “IMU-based smartphone-to-vehicle positioning,” *IEEE Transactions on Intelligent Vehicles.*, vol. 1, no. 2, pp. 139-147, Jul. 2016.
- [9] P. Aggarwal, Z. Syed, A. Noureldin, and N. El-Sheimy, *MEMS-based integrated navigation*, Norwood, MA, USA: Artech House, 2010.
- [10] L. Yang, Y. Li, Y. Wu, and C. Rizos, “An enhanced MEMS-INS/GNSS integrated system with fault detection and exclusion capability for land vehicle navigation in urban areas,” *GPS Solutions.*, vol. 18, no. 4, pp. 593-603, 2014.
- [11] A. Aboseeken, U. Iqbal, A. Noureldin, and M. J. Korenberg, “A novel multi-level integrated navigation system for challenging GNSS environments,” *IEEE Transactions on Intelligent Transportation Systems.*, vol. 22, no. 8, pp. 4838-4852, Aug. 2021.
- [12] A. Aboseeken, A. Noureldin, and M. J. Korenberg, “Improving the RIIS/GNSS land-vehicles integrated navigation system using magnetic azimuth updates,” *IEEE Transactions on Intelligent Transportation Systems.*, vol. 21, no. 3, pp. 1250-1263, Mar. 2020.

- [13] P. R. M. de Araujo, M. Elhabiby, S. Givigi, and A. Noureldin, "A Novel Method for Land Vehicle Positioning: Invariant Kalman Filters and Deep-Learning-Based Radar Speed Estimation," *IEEE Transactions on Intelligent Vehicles.*, vol. 8, no. 9, pp. 4275-4286, Sept. 2023.
- [14] S. Teng et al., "FusionPlanner: A multi-task motion planner for mining trucks via multi-sensor fusion", *Mechanical Systems and Signal Processing*, vol. 208, p. 111051, 2024.
- [15] M. Ramezani and K. Khoshelham, "Vehicle positioning in GNSS-deprived urban areas by stereo visual-inertial odometry," *IEEE Transactions on Intelligent Vehicles.*, vol. 3, no. 2, pp. 208-217, Jun. 2018.
- [16] S. Si, Y. Huang, Y. Nie, L. Xiao, D. Zhao, B. Dai, and Y. Zhang, "TOM-odometry: A generalized localization framework based on topological Map and Odometry," *IEEE Transactions on Aerospace and Electronic Systems.*, vol. 59, no. 3, pp. 2713-2732, June. 2023.
- [17] M. Brossard, A. Barrau, and S. Bonnabel, "AI-IMU dead-reckoning," *IEEE Transactions on Intelligent Vehicles.*, vol. 5, no. 4, pp. 585-595, Dec. 2020.
- [18] L. Cong, S. Yue, H. Qin, B. Li, and J. Yao, "Implementation of a MEMS-based GNSS/INS integrated scheme using supported vector machine for land vehicle navigation," *IEEE Sensors Journal.*, vol. 20, no. 23, pp. 14423-14435, Dec. 2020.
- [19] B. Or and I. Klein, "A hybrid model and learning based adaptive navigation filter," *IEEE Transactions on Instrumentation and Measurement.*, vol. 71, pp. 1-11, 2022.
- [20] S. Taghizadeh and R. Safabakhsh, "An integrated INS/GNSS system with an attention-based hierarchical LSTM during GNSS outage," *GPS Solution.*, vol. 27, no. 2, pp. 1-12, Feb. 2023.
- [21] Y. Hu, X. Li, D. Kong, K. Wei, P. Ni, and J. Hu, "A Reliable Position Estimation Methodology Based on Multi-Source Information for Intelligent Vehicles in Unknown Environment," *IEEE Transactions on Intelligent Vehicles.*, vol. 9, no. 1, pp. 1667-1680, Jan. 2024.
- [22] Y. Li, X. Niu, Q. Zhang, Y. Cheng, and C. Shi, "Observability analysis of non-holonomic constraints for land-vehicle navigation systems," in *Proceedings of the 25th International Technical Meeting of the Satellite Division of The Institute of Navigation. (ION GNSS)*, 2012, pp. 1521-1529.
- [23] L. Han, Z. Shi, J. Song, and H. Wang, "Vehicle Positioning Algorithm Based on NHC/Virtual-MINS/OD," *IEEE Transactions on Vehicular Technology.*, vol. 71, no. 5, pp. 4764-4775, May. 2022.
- [24] C. Kilic, N. Ohi, Y. Gu, and J. Gross, "Slip-based autonomous ZUPT through Gaussian process to improve planetary rover localization," *IEEE Robotics and Automation Letters.*, vol. 6, no. 3, pp. 4782-4789, Jul. 2021.
- [25] A. Ramanandan, A. Chen and J. A. Farrell, "Inertial navigation aiding by stationary updates," *IEEE Transactions on Intelligent Transportation Systems.*, vol. 13, no. 1, pp. 235-248, Mar. 2012.
- [26] C.-Y. Liu, C.-A. Lin, K.-W. Chiang, S.-C. Huang, C.-C. Chang, and J.-M. Cai, "Performance evaluation of real-time MEMS INS/GPS integration with ZUPT/ZIHR/NHC for land navigation," in *12th International Conference on ITS Telecommunications.*, Nov. 2012, pp. 584-588.
- [27] Q. Fu, Y. Liu, Z. Liu, S. Li, and B. Guan, "High-accuracy SINS/LDV integration for long-distance land navigation," *IEEE/ASME Transactions on Mechatronics.*, vol. 23, no. 6, pp. 2952-2962, Dec. 2018.
- [28] Q. Zhang, Y. Hu, S. Li, T. Zhang, and X. Niu, "Mounting parameter estimation from velocity vector observations for land vehicle navigation," *IEEE Transactions on Industrial Electronics.*, vol. 69, no. 4, pp. 4234-4244, Apr. 2022.
- [29] Q. Chen, Q. Zhang, and X. Niu, "Estimate the pitch and heading mounting angles of the IMU for land vehicular GNSS/INS integrated system," *IEEE Transactions on Intelligent Transportation Systems.*, vol. 22, no. 10, pp. 1-13, Oct. 2020.
- [30] Q. Zhang, Y. Hu, and X. Niu, "Required lever arm accuracy of non-holonomic constraint for land vehicle navigation," *IEEE Transactions on Vehicular Technology.*, vol. 69, no. 8, pp. 8305-8316, Aug. 2020.
- [31] S. Du, F. Zhu, Z. Wang, Y. Huang, and Y. Zhang, "A Novel Lie Group Framework-based Students t Robust Filter and Its Application to IN-S/DVL Tightly Integrated Navigation," *IEEE Transactions on Instrumentation and Measurement*, Early Access, doi: 10.1109/TIM.2024.3379400.
- [32] E. Vinande, P. Axelrad, and D. Akos, "Mounting-angle estimation for personal navigation devices," *IEEE Transactions on Vehicular Technology*, vol. 59, no. 3, pp. 1129-1138, Mar. 2010.
- [33] Y. Wu, C. Goodall, and N. El-Sheimy, "Self-calibration for IMU /odometer land navigation:Simulation and test results," in *Proceedings of the International Technical Meeting of The Institute of Navigation.*, 2010, pp. 839-849.
- [34] P.-J. Huber, *Robust Statistics*, New York, NY, USA: Wiley 1981.
- [35] B. Chen, X. Liu, H. Zhao, and J. C. Principe, "Maximum correntropy Kalman filter," *Automatica*, vol. 76, no. 2, pp. 70-77, Feb. 2017.
- [36] Y. L. Huang, Y. G. Zhang, Y. X. Zhao and J. Chambers, "A novel robust Gaussian-Student's *t* mixture distribution based Kalman filter," *IEEE Transactions on Signal Processing.*, vol. 67, no. 13, pp. 3606-3620, Jul. 2019.
- [37] PSINS. Available: <http://www.psins.org.cn/sy>. Accessed on: Oct 12, 2023.
- [38] S. Du, Y. Huang, B. Lin, J. Qian, and Y. Zhang, "A Lie Group Manifold-Based Nonlinear Estimation Algorithm and Its Application to Low-Accuracy SINS/GNSS Integrated Navigation," *IEEE Transactions on Instrumentation and Measurement.*, vol. 71, pp. 1-27, Mar. 2022.
- [39] A. Barrau and S. Bonnabel, "Invariant kalman filtering," *Annual Review of Control, Robotics, and Autonomous Systems.*, vol. 1, no. 1, pp. 237-257, May. 2018.
- [40] W. Ouyang, Y. Wu, and H. Chen, "INS odometer land navigation by accurate measurement modeling and multiple-model adaptive estimation," *IEEE Transactions on Aerospace and Electronic Systems.*, vol. 57 no. 1 pp. 245-262, Feb. 2021.
- [41] Y. Huang, Y. Zhang, Z. Wu, N. Li, and J. A. Chambers, "A novel adaptive Kalman filter with inaccurate process and measurement noise covariance matrices," *IEEE Transactions on Automatic Control.*, vol. 63, no. 2, pp. 594-601, Sep. 2018.
- [42] C. Pan, J. X. Gao, Z. K. Li, N. J. Qian, and F. C. Li, "Multiple fading factors-based strong tracking variational Bayesian adaptive Kalman filter," *Measurement.*, vol. 176, 2021, Art. no. 109139.

APPENDIX

A. Proofs of Theorem 1

In order to construct the SSM of the mounting error angle, it is first necessary to establish the VDR state update equation based on the posteriori SINS/GNSS straight-driving data. For the *u*-frame autonomous vehicles, the incremental distance Δs_k^u is defined as

$$\Delta s_k^u = \int_{t_{k-1}}^{t_k} \mathbf{v}^u(t) dt \quad (79)$$

where for the right-front-up frame, the incremental distance $\Delta s_k^u = [0, \Delta s_k, 0]$, and $\mathbf{v}^u(t) = [0, v^u, 0]$ denotes the *u*-frame velocity of autonomous vehicle, and it is formulated as follows

$$v^u = \sqrt{\hat{v}_R^2 + \hat{v}_F^2 + \hat{v}_U^2} \quad (80)$$

where \hat{v}_R , \hat{v}_F , and \hat{v}_U denote the *b* frame velocity of right, front, and up, respectively, and they can be obtained from the posteriori SINS/GNSS navigation state data. Then, the VDR position $\mathbf{r}_{\text{vdr}}^n$ updated equation can be constructed based on the the incremental distance Δs_k^u , and it is formulated as follows

$$\mathbf{r}_{\text{vdr},k}^n = \mathbf{r}_{\text{vdr},k-1}^n + \mathbf{C}_b^n \mathbf{C}_u^b \Delta s_k^u \quad (81)$$

Accordingly, the VDR position update equation with error is formulated as follows

$$\tilde{\mathbf{r}}_{\text{vdr},k}^n = \tilde{\mathbf{r}}_{\text{vdr},k-1}^n + \tilde{\mathbf{C}}_b^n \tilde{\mathbf{C}}_u^b \Delta s_k^u \quad (82)$$

where

$$\tilde{\mathbf{r}}_{\text{vdr},k}^n = \mathbf{r}_{\text{vdr},k}^n + \delta \mathbf{r}_{\text{vdr},k}^n \quad (83)$$

$$\tilde{\mathbf{C}}_b^n = (\mathbf{I}_3 - \boldsymbol{\phi}_{\text{ma}}^n \times) \mathbf{C}_b^n \quad (84)$$

$$\tilde{\mathbf{C}}_u^b = (\mathbf{I}_3 - \boldsymbol{\alpha}_{\text{ma}} \times) \mathbf{C}_u^b \quad (85)$$

Then, based on the definition in (22), the right invariant position error is given as follows

$$\boldsymbol{\zeta}_{\text{ma}}^R = -\delta \mathbf{r}_{\text{vdr}}^n + (\mathbf{r}_{\text{vdr}}^n \times) \boldsymbol{\phi}_{\text{ma}}^n \quad (86)$$

and (83) can be further represented as follows

$$\tilde{\mathbf{r}}_{\text{vdr},k}^n = \mathbf{r}_{\text{vdr},k}^n - \zeta_{\text{ma},k}^R + (\mathbf{r}_{\text{vdr},k}^n \times) \phi_{\text{ma}}^n \quad (87)$$

Therefore, the right invariant error-based VDR position update equation is formulated as follows

$$\begin{aligned} \tilde{\mathbf{r}}_{\text{vdr},k}^n &= \mathbf{r}_{\text{vdr},k-1}^n - \zeta_{\text{ma},k-1}^R + (\mathbf{r}_{\text{vdr},k-1}^n \times) \phi_{\text{ma}}^n \\ &\quad + \tilde{\mathbf{C}}_b^n \tilde{\mathbf{C}}_u^b \Delta \mathbf{s}_k^u \end{aligned} \quad (88)$$

Substituting (84), (85) into (88) gives

$$\begin{aligned} \tilde{\mathbf{r}}_{\text{vdr},k}^n &= \mathbf{r}_{\text{vdr},k-1}^n - \zeta_{\text{ma},k-1}^R + (\mathbf{r}_{\text{vdr},k-1}^n \times) \phi_{\text{ma}}^n \\ &\quad + \mathbf{C}_b^n \mathbf{C}_u^b \Delta \mathbf{s}_k^u - \mathbf{C}_b^n \mathbf{C}_u^b (\Delta \mathbf{s}_k^u \times) \alpha_{\text{ma}} + (\mathbf{C}_b^n \mathbf{C}_u^b \Delta \mathbf{s}_k^u) \\ &\quad \times \phi_{\text{ma}}^n \end{aligned} \quad (89)$$

Then, subtracting (81) from (89) gives

$$\begin{aligned} -\zeta_{\text{ma},k}^R + (\mathbf{r}_{\text{vdr},k}^n \times) \phi_{\text{ma}}^n &= -\zeta_{\text{ma},k-1}^R + (\mathbf{r}_{\text{vdr},k-1}^n \times) \phi_{\text{ma}}^n \\ &\quad - \mathbf{C}_b^n \mathbf{C}_u^b (\Delta \mathbf{s}_k^u \times) \alpha_{\text{ma}} + (\mathbf{C}_b^n \mathbf{C}_u^b \Delta \mathbf{s}_k^u) \\ &\quad \times \phi_{\text{ma}}^n \end{aligned} \quad (90)$$

and (90) can also be summarized as follows

$$\begin{aligned} -\zeta_{\text{ma},k}^R &= -\zeta_{\text{ma},k-1}^R - (\Delta \mathbf{s}_k^n \times) \phi_{\text{ma}}^n - \mathbf{C}_b^n \mathbf{C}_u^b (\Delta \mathbf{s}_k^u \times) \alpha_{\text{ma}} \\ &\quad + (\Delta \mathbf{s}_k^n \times) \phi_{\text{ma}}^n \\ &= -\zeta_{\text{ma},k-1}^R - \mathbf{C}_b^n \mathbf{C}_u^b \mathbf{M}^R \begin{bmatrix} \alpha_x \\ \alpha_z \end{bmatrix} \end{aligned} \quad (91)$$

Therefore, the proposed right invariant error-based VDR position error equation is given by

$$\zeta_{\text{ma},k}^R = \zeta_{\text{ma},k-1}^R + \mathbf{C}_b^n \mathbf{C}_u^b \mathbf{M}^R \begin{bmatrix} \alpha_x \\ \alpha_z \end{bmatrix} \quad (92)$$

where

$$\mathbf{M}^R = \begin{bmatrix} 0 & \Delta s_k \\ 0 & 0 \\ -\Delta s_k & 0 \end{bmatrix} \quad (93)$$

and Δs_k is calculated by (79)-(80), which is formulated as $\Delta s_k = \mathbf{v}^u dt$, and based on (92), the corresponding SSM can be defined as follows

$$\mathbf{x}_{\text{ma},k|k-1}^R = \Phi_{k|k-1}^R \mathbf{x}_{\text{ma},k-1}^R + \Gamma_{k-1}^R \boldsymbol{\sigma}_{k-1} \quad (94)$$

where

$$\Phi_{k|k-1}^R = \begin{bmatrix} \mathbf{I}_3 & \mathbf{C}_b^n \mathbf{C}_u^b \mathbf{M}^R & \mathbf{0}_3 \\ \mathbf{0}_2 & \mathbf{I}_2 & \mathbf{0}_2 \\ \mathbf{0}_3 & \mathbf{0}_3 & \mathbf{I}_3 \end{bmatrix}, \Gamma_{k-1}^R = \begin{bmatrix} \mathbf{0}_{3 \times 5} \\ \mathbf{I}_5 \end{bmatrix} \quad (95)$$

where $\boldsymbol{\sigma}_{k-1}$ denote the Gaussian noise, and the right invariant error is defined as

$$\mathbf{x}_{\text{ma}}^R = [\zeta_{\text{ma}}^R, \alpha_{\text{ma}}, \phi_{\text{ma}}^n]^T \quad (96)$$

where ζ_{ma}^R , α_{ma} , and ϕ_{ma}^n denote the right invariant position error, the mounting error angle, and misalignment angle, respectively. In addition, based on the definition of right invariant position error in (86), the VDR measurement equation is also formulated as follows

$$\mathbf{r}_{\text{vdr}}^n - \mathbf{r}_{\text{sins/gnss}}^n = -\zeta_{\text{ma}}^n + (\mathbf{r}_{\text{vdr}}^n \times) \phi_{\text{ma}}^n \quad (97)$$

where $\mathbf{r}_{\text{sins/gnss}}^n$ denotes the posteriori SINS/GNSS position vector, and then it can be summarized as follows

$$\mathbf{z}_{\text{ma},k}^R = \mathbf{H}_{\text{ma}}^R \mathbf{x}_{\text{ma},k|k-1}^R + \boldsymbol{\nu}_{\text{ma}}^R \quad (98)$$

where $\boldsymbol{\nu}_{\text{ma}}^R$ denotes measurement noise, and the measurement innovation $\mathbf{z}_{\text{ma},k}^R$ and the measurement matrix \mathbf{H}_{ma}^R are formulated as follows, respectively

$$\begin{aligned} \mathbf{z}_{\text{ma},k}^R &= \mathbf{r}_{\text{vdr}}^n - \mathbf{r}_{\text{sins/gnss}}^n, \\ \mathbf{H}_{\text{ma}}^R &= [-\mathbf{I}_3 \ \mathbf{0}_{3 \times 2} \ (\mathbf{r}_{\text{vdr}}^n \times)] \end{aligned} \quad (99)$$

In conclusion, the constructed RIEKF-based VDR is summarized as (94)-(99).

B. Proofs of Theorem 2

In order to derive the left invariant error-based NHC measurement equation, the NHC velocity equation is formulated as follows

$$\mathbf{v}_{\text{nhc}}^u = \hat{\mathbf{C}}_b^u \mathbf{C}_n^b \mathbf{v}_{\text{sins}}^n + \hat{\mathbf{C}}_b^u (\omega_{nb}^b \times \hat{\mathbf{l}}^b) \quad (100)$$

where $\hat{\mathbf{C}}_b^u$ and $\hat{\mathbf{l}}^b$ denote the estimated mounting angle matrix and lever arm, respectively, and then it is also obtained as

$$\tilde{\mathbf{v}}_{\text{nhc}}^u = \hat{\mathbf{C}}_b^u \tilde{\mathbf{C}}_n^b \tilde{\mathbf{v}}_{\text{sins}}^n + \hat{\mathbf{C}}_b^u (\tilde{\omega}_{nb}^b \times \hat{\mathbf{l}}^b) \quad (101)$$

Furthermore, (101) can be represented as follows

$$\begin{aligned} \mathbf{v}_{\text{nhc}}^u + \delta \mathbf{v}_{\text{nhc}}^u &= \hat{\mathbf{C}}_b^u \tilde{\mathbf{C}}_n^b \mathbf{C}_n^b (\mathbf{v}_{\text{sins}}^n + \delta \mathbf{v}_{\text{sins}}^n) \\ &\quad + \hat{\mathbf{C}}_b^u (\omega_{nb}^b + \delta \omega_{nb}^b) \times \hat{\mathbf{l}}^b \end{aligned} \quad (102)$$

For the left invariant velocity error, it is defined as follows

$$\delta \mathbf{v}_{\text{sins}}^n = \delta \mathbf{v}_{ib}^n - (\omega_{ie}^n \times) \delta \mathbf{r}_{ib}^n \quad (103)$$

and then, it can be further formulated as follows

$$\delta \mathbf{v}_{\text{sins}}^n = -\mathbf{C}_b^n \zeta_v^b + (\omega_{ie}^n \times) \mathbf{C}_b^n \zeta_r^b \quad (104)$$

Substituting $\tilde{\mathbf{C}}_n^b \mathbf{C}_b^n = (\mathbf{I}_3 + \phi_{\text{nav}}^b)$ and (104) into (102) results in

$$\begin{aligned} \mathbf{v}_{\text{nhc}}^u + \delta \mathbf{v}_{\text{nhc}}^u &\approx \hat{\mathbf{C}}_b^u \mathbf{C}_n^b \mathbf{v}_{\text{sins}}^n + \hat{\mathbf{C}}_b^u (\omega_{nb}^b \times) \hat{\mathbf{l}}^b - \hat{\mathbf{C}}_b^u \zeta_r^b \\ &\quad + \hat{\mathbf{C}}_b^u (\mathbf{C}_n^b \omega_{ie}^n) \times \zeta_r^b - \hat{\mathbf{C}}_b^u (\mathbf{C}_n^b \mathbf{v}_{\text{sins}}^n) \times \phi_{\text{nav}}^b \\ &\quad - \hat{\mathbf{C}}_b^u (\mathbf{l}^b \times) \delta \omega_{ib}^b \end{aligned} \quad (105)$$

and then

$$\begin{aligned} \delta \mathbf{v}_{\text{nhc}}^u &= -\hat{\mathbf{C}}_b^u \zeta_v^b + \hat{\mathbf{C}}_b^u (\mathbf{C}_n^b \omega_{ie}^n) \times \zeta_r^b - \hat{\mathbf{C}}_b^u (\mathbf{C}_n^b \mathbf{v}_{\text{sins}}^n) \times \phi_{\text{nav}}^b \\ &\quad - \hat{\mathbf{C}}_b^u (\mathbf{l}^b \times) \delta \omega_{ib}^b \end{aligned} \quad (106)$$

Therefore, (106) can be summarized as follows

$$\mathbf{z}_{\text{nhc},k}^L = \mathbf{H}_{\text{nhc}}^L \mathbf{x}_{\text{nav},k|k-1}^L + \boldsymbol{\nu}_{\text{nhc}}^L \quad (107)$$

where $\mathbf{z}_{\text{nhc},k}^L$ and $\boldsymbol{\nu}_{\text{nhc}}^L$ denote the measurement innovation and measurement noise, respectively, and the left invariant error-based NHC measurement matrix $\mathbf{H}_{\text{nhc}}^L$ is formulated as follows

$$\mathbf{H}_{\text{nhc}}^L = \begin{bmatrix} \mathbf{h}_{\{1,1\}}^L & \mathbf{h}_{\{1,2\}}^L & \mathbf{h}_{\{1,3\}}^L & \mathbf{h}_{\{1,4\}}^L & \mathbf{0}_{1 \times 3} \\ \mathbf{h}_{\{2,1\}}^L & \mathbf{h}_{\{2,2\}}^L & \mathbf{h}_{\{2,3\}}^L & \mathbf{h}_{\{2,4\}}^L & \mathbf{0}_{1 \times 3} \end{bmatrix} \quad (108)$$

where

$$\begin{cases} \mathbf{h}_{\{1,1\}}^L = -\hat{\mathbf{C}}_b^u (\mathbf{v}_{\text{sins}}^b) \times (1,:) \\ \mathbf{h}_{\{1,2\}}^L = -\hat{\mathbf{C}}_b^u (1,:) \\ \mathbf{h}_{\{1,3\}}^L = \hat{\mathbf{C}}_b^u (\mathbf{C}_n^b \boldsymbol{\omega}_{ie}^n) \times (1,:) \\ \mathbf{h}_{\{1,4\}}^L = -\hat{\mathbf{C}}_b^u (\hat{\mathbf{l}}^b \times) (1,:) \end{cases} \quad (109)$$

and

$$\begin{cases} \mathbf{h}_{\{2,1\}}^L = -\hat{\mathbf{C}}_b^u (\mathbf{v}_{\text{sins}}^b) \times (3,:) \\ \mathbf{h}_{\{2,2\}}^L = -\hat{\mathbf{C}}_b^u (3,:) \\ \mathbf{h}_{\{2,3\}}^L = \hat{\mathbf{C}}_b^u (\mathbf{C}_n^b \boldsymbol{\omega}_{ie}^n) \times (3,:) \\ \mathbf{h}_{\{2,4\}}^L = -\hat{\mathbf{C}}_b^u (\hat{\mathbf{l}}^b \times) (3,:) \end{cases} \quad (110)$$



Siyuan Du received the B.S. and M.S. degrees in measurement and control technology and instruments from the School Instrument and Electronics, North University of China, Taiyuan, China, in 2015 and 2018, respectively. He is currently pursuing the Ph.D. degree in Automation from the Department of Intelligent Science and Engineering, Harbin Engineering University. His research interests include inertial navigation, integrated navigation, and information fusion.



Yulong Huang (Senior Member, IEEE) received the B.S. degree in Automation from the College of Automation, Harbin Engineering University, Harbin, China, in 2012. He received the Ph.D. degree in control science and engineering from the College of Automation, Harbin Engineering University, Harbin, China, in 2018. From Nov. 2016 to Nov. 2017, he was a visiting graduate researcher at the Electrical Engineering Department of Columbia University, New York, USA. From Dec. 2019 to Dec. 2021, he was associated with the Department of Mechanical

Engineering, City University of Hong Kong, as a Hong Kong Scholar.

He is a Full Professor of navigation, guidance, and control, and Vice Dean of College of Intelligent Systems Science and Engineering at Harbin Engineering University (HEU) in China. His current research interests include state estimation, intelligent information fusion and their applications in navigation technology, such as inertial navigation, integrated navigation, intelligent navigation, and cooperative navigation. Currently, he serves as an Associate Editor for the IEEE TRANSACTIONS ON AEROSPACE AND ELECTRONIC SYSTEMS, for the IEEE TRANSACTIONS ON INSTRUMENTATION AND MEASUREMENT, and for the IEEE SENSORS JOURNAL, and a Youth Editor for the IEEE/CAA JOURNAL OF AUTOMATICA SINICA (JAS), for the JOURNAL OF MARINE SCIENCE AND APPLICATION, for the UNMANNED SYSTEMS TECHNOLOGY, for the JOURNAL OF UNMANNED UNDERSEA SYSTEMS, for the NAVIGATION POSITIONING AND TIMING.

He was the recipient of the 2018 IEEE Barry Carlton Award from IEEE TRANSACTIONS ON AEROSPACE AND ELECTRONIC SYSTEMS in 2022, the Honorable Mention of 2017 IEEE Barry Carlton Award from IEEE TRANSACTIONS ON AEROSPACE AND ELECTRONIC SYSTEMS in 2021, the Best Student Paper Award of 2023 IEEE International Conference on Mechatronics and Automation (IEEE ICMA 2023), and the Best Paper Award of 2021 International Conference on Autonomous Unmanned Systems (ICAUS 2021). He was also the recipient of the 11th China Youth Science and Technology Innovation Awards in 2018, the excellent doctoral thesis from Chinese Association of Automation (CAA) in 2019, the Wu Wen-Jun AI Excellent Youth Scholar Award in 2021, the First Prize of Natural Science Award of Chinese Association of Automation (Ranked the 2nd) in 2021, and he was selected into the sixth Young Elite Scientists Sponsorship Program by China Association for Science and Technology in 2020. He was an outstanding Associate Editor and Reviewer for the IEEE TRANSACTIONS ON INSTRUMENTATION AND MEASUREMENT.



Weisong Wen (Member, IEEE) received a BEng degree in Mechanical Engineering from Beijing Information Science and Technology University (BISTU), Beijing, China, in 2015, and an MEng degree in Mechanical Engineering from the China Agricultural University, in 2017. After that, he received a PhD degree in Mechanical Engineering from The Hong Kong Polytechnic University (PolyU), in 2020. He was also a visiting PhD student with the Faculty of Engineering, University of California, Berkeley (UC Berkeley) in 2018. Before joining PolyU as an

Assistant Professor in 2023, he was a Research Assistant Professor at AAE of PolyU since 2021. He has published 30 SCI papers and 40 conference papers in the field of GNSS (ION GNSS+) and navigation for Robotic systems (IEEE ICRA, IEEE ITSC), such as autonomous driving vehicles. He won the innovation award from TechConnect 2021, the Best Presentation Award from the Institute of Navigation (ION) in 2020, and the First Prize in Hong Kong Section in Qianhai-Guangdong-Macao Youth Innovation and Entrepreneurship Competition in 2019 based on his research achievements in 3D LiDAR aided GNSS positioning for robotics navigation in urban canyons. The developed 3D LiDAR-aided GNSS positioning method has been reported by top magazines such as Inside GNSS and has attracted industry recognition with remarkable knowledge transfer.



Yonggang Zhang (Senior Member, IEEE) received the B.S. and M.S. degrees from the Department of Automation, Harbin Engineering University, Harbin, China, in 2002 and 2004, respectively. He received his Ph.D. degree in Electronic Engineering from Cardiff University, UK in 2007 and worked as a Post-Doctoral Fellow at Loughborough University, UK from 2007 to 2008 in the area of adaptive signal processing. Currently, he is a Professor of navigation, guidance, and control in Harbin Engineering University (HEU) in China. His current research interests include signal processing, information fusion and their applications in navigation technology, such as fiber optical gyroscope, inertial navigation and integrated navigation.